THE EFFECT OF P_2O_5 ON THE DEVITRIFICATION OF LEAD SILICATE GLASSES

Dissertation for the Degree of Ph. D.

MICHIGAN STATE UNIVERSITY
SANDRA HAARALA CARR

1977

This is to certify that the

thesis entitled

THE EFFECT OF P_2O_5 ON THE DEVITRIFICATION
OF LEAD SILICATE GLASSES

presented by

Sandra Haarala Carr

has been accepted towards fulfillment
of the requirements for

Ph.D. degree in Materials Science

K. N. Subramanian

Major professor

Date February 25 1977

ABSTRACT

THE EFFECT OF P_2O_5 ON THE DEVITRIFICATION OF LEAD SILICATE GLASSES

By

Sandra Haarala Carr

The effect of P_2O_5 on the devitrification of binary lead silicate glasses containing 64 mole percent and 59 mole percent PbO was studied. Glasses containing 64 mole percent PbO were prepared with P_2O_5 concentrations of 0.5 and 1.0 mole percent, and glasses containing 59 mole percent PbO were prepared with P_2O_5 concentrations of 0.1 and 0.5 mole percent. These glasses were devitrified at temperatures of 400°C, 450°C, 500°C, and 550°C. The crystallization products were determined by x-ray analysis, and the crystal growth rates and microstructures were determined by electron and optical microscopy.

The major product of crystallization for all compositions of glasses studied was a polymorph of $3PbO \cdot 2SiO_2$. The 64 mole percent PbO glasses contained a low temperature polymorph of $2PbO \cdot SiO_2$ as an additional phase, and the 59 mole percent PbO glasses contained a polymorph of $PbO \cdot SiO_2$.

Concentrations of 0.5 and 1.0 mole percent P_2O_5 promoted internal crystallization in the form of spherulites. The maximum nucleation rates for spherulitic crystallization occurred at 400°C. They were determined to be 3.29×10^6 spherulites-cm^{-3}-min^{-1} and 2.10×10^4 spherulites-cm^{-3}-min^{-1} for the 64 mole percent PbO glass containing 1.0 and 0.5 mole percent P_2O_5, respectively; and about 3×10^5 spherulites-cm^{-3}-min^{-1} for the 59 mole percent PbO glass containing 0.5 mole percent P_2O_5. Spherulitic growth rates were constant

with time fo

tion energy

lite develop

characteris

morphology

textures at

litic growth

well for the

with time for isothermal heat treatments. The experimental activation energy for spherulitic growth was about 84 kcal/mole. Spherulite development followed the sheaf-to-spherulite sequence that is characteristic of spherulites in other materials. The spherulite morphology, which varied with temperature, displayed coarse, open textures at 550^{0}C and fine textures at 400^{0}C. The model of spherulitic growth developed by Keith and Padden[45] accounts reasonably well for the spherulitic growth mode.

TH

Departm

THE EFFECT OF P_2O_5 ON THE DEVITRIFICATION OF LEAD SILICATE GLASSES

By

Sandra Haarala Carr

A DISSERTATION

Submitted to
Michigan State University
in partial fulfillment of the requirements
for the degree of

DOCTOR OF PHILOSOPHY

Department of Metallurgy, Mechanics, and Materials Science

1977

to the memory of my father

I wo

are respo

my

ingness to

the

Donald J.

and suppo

Dr.

who go out

students;

my p

faith and s

my h

ness and a

and,

and encour

ACKNOWLEDGMENTS

I would like to give special thanks to the following people, who are responsible in one way or another for the completion of this work:

my advisor, Dr. K. N. Subramanian, for his guidance and willingness to help, regardless of the time of day (or night);

the faculty and staff of the MMM Department, especially Dr. Donald J. Montgomery and Dr. Robert Summitt, for their friendship and support;

Dr. Gary Hooper and his associates at the Electron Optics Lab, who go out of their way to assist and co-operate with campus graduate students;

my parents, William and Henrietta Haarala, for their unfailing faith and support;

my husband, Dale, for his resourceful "handy-man" innovativeness and amazing ability to live with a graduate student wife;

and, finally, my fellow graduate students for their friendship, and encouragement, over the years.

LIST OF TABL
LIST OF FIGUR
Chapter
I. INTRO
II. THEO
2.1 C
2.2 G
2.3 C
III. THE L
3.1 C
3.2 R
IV. EXPE
4.1 C
4.2 D
4.3 M
V. RESU
5.1 C
5.2 P
5.3 S
5.4 S
5.5 E
VI. SUMM
APPENDIX
A. HIST
IN DI
LIST OF REF

TABLE OF CONTENTS

	Page
LIST OF TABLES	v
LIST OF FIGURES	vi
Chapter	
I. INTRODUCTION	1
II. THEORY	3
2.1 Classical Nucleation Theory	6
2.2 Growth Processes	10
2.3 Crystallization in Glass-Forming Systems	12
III. THE LEAD SILICATE SYSTEM	16
3.1 Compound Formation	16
3.2 Rate of Crystallization	23
IV. EXPERIMENTAL PROCEDURE	26
4.1 Glass Preparation	26
4.2 Devitrification of Glasses	28
4.3 Methods of Observation and Analysis	29
V. RESULTS AND DISCUSSION	33
5.1 Crystallization Products	33
5.2 Microstructure of Glasses	43
5.3 Spherulitic Growth Rate	58
5.4 Spherulitic Morphology	66
5.5 Role of P_2O_5	75
VI. SUMMARY	83
APPENDIX	
A. HISTOGRAMS OF SPHERULITE POPULATIONS IN DEVITRIFIED GLASSES	85
LIST OF REFERENCES	108

LIST OF TABLES

Table		Page
1.	The d-spacings and relative intensities of the x-ray spectra for the major crystalline phase	36
2.	The d-spacings and relative intensities of the x-ray spectra for the low temperature phase in devitrified 70-30 glass	37
3.	The d-spacings and relative intensities of the x-ray spectra for the secondary crystalline phase in devitrified 60-40 and 60-40-0.5 glass	44
4.	Crystal growth rate as a function of temperature and glass composition	64

LIST OF FIGURES

Figure		Page
1.	Rates of nucleation and growth for viscous liquids as a function of the degree of undercooling . . .	5
2.	Variation of Gibbs Free Energy with radius for condensation of a spherical droplet in a supersaturated vapor	8
3.	Reaction paths between the initial glass and the final glass-ceramic	14
4.	Phase diagram of the lead silicate system by Geller et al.	17
5.	Phase diagram of the lead silicate system by Ott and McLaren	22
6.	Phase diagram of the lead silicate system by Smart and Glasser	24
7.	Microtome set-up for sectioning glass	31
8.	X-ray diffraction spectra of 70-30 glass devitrified for (a) 7 days at 400°C, (b) 6 days at 450°C, (c) 3 days at 500°C, and (d) 3 days at 550°C	34
9.	X-ray diffraction spectra of 70-30-1.0 glass devitrified for (a) 10 days at 400°C and (b) 3 days at 550°C	40
10.	X-ray diffraction spectra of (a) 70-30 glass devitrified for 3 days at 550°C and (b) 70-30-1.0 glass devitrified for 3 days at 550°C	41
11.	X-ray diffraction spectra of 60-40 glass devitrified for (a) 18 days at 400°C, (b) 6 days at 450°C, (c) 3 days at 500°C, and (d) 3 days at 550°C	42
12.	X-ray diffraction spectra of 60-40-0.5 glass devitrified for (a) 18 days at 400°C and (b) 3 days at 550°C	45

Figure Page

13. Electron micrographs of replicas of quenched (a) 70-30 glass, (b) 70-30-0.5 glass, and (c) 70-30-1.0 glass 46

14. Electron micrograph of radial crystal growth pattern in quenched 70-30-0.5 glass 48

15. Electron micrograph of phase separated region between crystalline growth front and matrix in quenched 70-30-0.5 glass 49

16. Micrographs of surface crystallites in (a) 70-30 glass, (b) 70-30-0.5 glass, and (c) 70-30-1.0 glass after devitrification at 400°C for 42 hours 50

17. Micrograph of surface crystals in 70-30-0.5 glass after devitrification for 1 hour at 400°C followed by 12 hours at 450°C 52

18. Micrographs of (a) 60-40 glass devitrified at 550°C for 1 hour and (b) 70-30 glass devitrified at 550°C for 72 hours 53

19. Microstructure of crystalline surface layer in (a) 60-40-0.1 glass devitrified for 1 hour at 550°C and (b) 60-40-0.5 glass devitrified for 72 hours at 550°C 55

20. Microstructures after devitrification at 550°C for 72 hours of (a) 60-40-0.5 glass and (b) 70-30-1.0 glass 56

21. Microstructure of 60-40-0.5 glass after devitrification at 500°C for 72 hours 57

22. Micrographs of spherulites in (a) 60-40-0.5 glass devitrified for 14 days at 400°C, (b) 70-30-0.5 glass devitrified for 8 days at 400°C, and (c) 70-30-1.0 glass devitrified for 4 days at 400°C 59

23. Growth curves for spherulites in 70-30-0.5 glass at (a) 400°C, (b) 450°C, (c) 500°C, and (d) 550°C . . 61

24. Growth curves for spherulites in 70-30-1.0 glass at (a) 400°C, (b) 450°C, (c) 500°C, and (d) 550°C . . 62

25. Growth curves for spherulites in 60-40-0.5 glass at (a) 400°C, (b) 450°C, (c) 500°C, and (d) 550°C . . 63

26. Graph of ln(crystal growth rate) versus the reciprocal of the absolute temperature 65

Figure Page

27. Spherulites grown at 550°C showing typical (a) sheaf, (b) bundle, and (c) hexagonal morphologies 67

28. Diagram of spherulite orientation 69

29. Micrograph of a spherulite in 70-30-0.5 glass after growth at 450°C 70

30. Electron micrograph of fibrous growth morphology in spherulites grown at 400°C in 70-30-0.5 glass 71

31. Micrograph of an early growth stage in a spherulite grown at 550°C 72

32. Electron micrograph of branching fibers in a spherulite grown at 550°C 73

33. Micrograph of a mature spherulite grown at 550°C . . . 74

34. Network of inter-spherulitic boundaries in a completely devitrified 70-30-0.5 glass 76

35. Free energy of an interface versus occupied fraction of surface sites 78

36. Electron micrograph of faceted crystal growth in a 60-40-0.1 glass after devitrification at 450°C for 1 hour 81

A.1. Histograms of spherulites grown in 70-30-0.5 glass at 400°C for (a) 2 days, (b) 3¼ days, (c) 4 days, (d) 5 days, (e) 6 days, and (f) 14 days 87

A.2. Histograms of spherulites grown in 70-30-1.0 glass at 400°C for (a) 2 days, (b) 3¼ days, and (c) 4 days 89

A.3. Histograms of spherulites grown in 60-40-0.5 glass at 400°C for (a) 14 days, (b) 18 days, (c) 25 days, and (d) 32 days 90

A.4. Histograms of spherulites grown in 70-30-0.5 glass at 450°C for (a) 200 min., (b) 240 min., (c) 360 min., (d) 480 min., and (e) 600 min., after a nucleation heat treatment of 1 hour at 400°C . . . 92

A.5. Histograms of spherulites grown in 70-30-1.0 glass at 450°C for (a) 200 min., (b) 275 min., (c) 480 min., (d) 600 min., and (e) 720 min. 94

Figure Page

A. 6. Histograms of spherulites grown in 60-40-0.5 glass at 450°C for (a) 720 min., (b) 1080 min., and (c) 1405 min. after a nucleation heat treatment of 1 hour at 400°C; and for (d) 1440 min., (e) 1680 min., and (f) 1920 min. after a nucleation heat treatment of 6 hours at 400°C 96

A. 7. Histograms of spherulites grown in 70-30-0.5 glass at 500°C for (a) 10 min., (b) 15 min., (c) 22 min., (d) 30 min., and (e) 37 min., after a nucleation heat treatment of 1 hour at 400°C 98

A. 8. Histograms of spherulites grown in 70-30-1.0 glass at 500°C for (a) 10 min., (b) 15 min., (c) 22 min., (d) 30 min., and (e) 37 min. 100

A. 9. Histograms of spherulites grown in 60-40-0.5 glass at 500°C for (a) 20 min., (b) 40 min., (c) 60 min., (d) 80 min., (e) 100 min., (f) 120 min., and (g) 140 min., after a nucleation heat treatment of 6 hours at 400°C 102

A. 10. Histograms of spherulites grown in 70-30-0.5 glass at 550°C for (a) 3 min. and (b) 5 min., after a nucleation heat treatment of 1 hour at 400°C 105

A. 11. Histograms of spherulites grown in 70-30-1.0 glass at 550°C for (a) 3 min., (b) 5 min., and (c) 10 min. 106

A. 12. Histograms of spherulites grown in 60-40-0.5 glass at 550°C for (a) 15 min., (b) 22 min., and (c) 30 min., after a nucleation heat treatment of 6 hours at 400°C . . 107

CHAPTER I
INTRODUCTION

The $PbO-SiO_2$ combination forms the basis for many industrially important polycomponent systems, including flint glasses, pottery glazes, enamels, and solder glasses for metal-to-glass seals. Much of the usefulness of this system is directly dependent upon its devitrification properties. Solder glasses, for example, require high fluidity and rapid devitrification at low to moderate temperatures. The lead silicate system, especially those compositions high in lead oxide content, has proven extremely useful for these applications.

In the lead silicate system, devitrification is rapid for compositions of high lead oxide content and usually starts at the glass surface and proceeds towards the interior. Devitrification via surface crystallization is often accompanied by sample deformation and cracking, and usually results in weak materials with degraded mechanical properties. If crystallization can be made to proceed by internal (or bulk) crystallization, however, the degradation of the mechanical properties can often be avoided. Recent work on the devitrification of glasses has shown that internal crystallization can sometimes be promoted if small amounts of nucleating agents are incorporated into the glass. Pavlushkin et al.[1,2,3] have investigated the effect of various nucleating agents, e.g. F, TiO_2, and P_2O_5, on the devitrification of lead silicate glasses with high lead oxide content, and in 1966 reported that P_2O_5 was the most effective catalyst for promoting internal crystallization in this system. According to their observations, crystallization proceeds through the following sequence: during cooling, phase separation occurs followed by the formation of crystalline nuclei which grow during subsequent heat treatment. In support of this mechanism is the

work of Vogel [4] who reported that glasses containing 60 mole percent PbO and 40 mole percent SiO_2 phase separate. In 1969, however, Shaw and Uhlmann [5] predicted, on the basis of their work on the density versus composition curves, that the most probable composition range for immiscibility in the lead silicate system was in the region from 0 to 50 mole percent PbO. The glasses studied by both Pavlushkin [1,2,3] and Vogel [4] were outside this composition range.

The purpose of this research was to determine the effect of P_2O_5 on the devitrification of lead silicate glasses of high PbO content. Two glass compositions were studied, one containing 59 mole percent PbO and the other containing 64 mole percent PbO. Investigations were aimed at determining the effect of P_2O_5 on

(1) the rate of crystal growth,

(2) the resultant crystal phases,

(3) the microstructure of the devitrified glasses, and

(4) the crystal morphology.

CHAPTER II
THEORY

The glassy state is a solid state characterized by the absence of molecular arrays with long range order. With many materials, it is difficult to achieve high enough cooling rates to prevent molecules from rearranging themselves into regular arrays with long range order. These materials crystallize upon solidification. With other materials, however, the time required for molecular rearrangement is long enough that it is possible to cool the system from the liquid state without crystallization occurring. Although many materials can be formed as glasses with rapid enough cooling rates, the phrase glass-forming materials is generally reserved for those materials which form glasses in bulk form when cooled at moderate rates from the liquid state. Thus, the tendency of a melt to form a glass upon cooling depends upon the interplay between (1) the rate at which it is cooled and (2) the kinetics of the crystallization processes involved. Materials with slow crystallization rates tend to form glasses easily.

The vitreous state is a metastable, not an equilibrium, state from which the materials would like to escape, via devitrification. If a sufficient amount of energy is available, the vitreous material can devitrify and transform into a crystalline material. The crystalline products formed are usually the equilibrium phases for the system, as determined by the phase diagram for the system.

Crystallization of a supercooled liquid usually starts with the formation of nuclei. It is, therefore, customary to view crystallization as a two-step process involving nucleation and growth. Formation of nuclei occurs during the nucleation stage. If the nuclei form spontaneously from the transforming phase, unaided by the

presence of foreign particles, then the process is termed homogeneous nucleation. If, on the other hand, nuclei formation is initiated by the presence of foreign particles, then the process is termed heterogeneous nucleation. The foreign particles may be anything present in the parent phase that causes it to be non-homogeneous, e.g. impurities such as dust or dirt, air bubbles, crystals of another phase, or even crystals of the same phase if they are added to the parent phase (instead of being nucleated from it). Crystal growth proceeds from these nuclei during the growth stage. The rate at which crystallization occurs is a function of both the nucleation and growth rates and is limited by the slower of the two processes. Either a low nucleation rate or a low growth rate can prevent crystallization from occurring on a reasonable time scale.

In studying the solubilities of materials, Ostwald [6] observed that some degree of undercooling from the equilibrium melt temperature always preceeded crystallization. Homogeneous crystallization seemed to be dependent upon the liquid's reaching some degree of supersaturation before crystallization could take place. From his observations, Ostwald postulated the existence of a metastable zone of supersaturation within which crystal nuclei could not form spontaneously. Experimental studies since then have been carried out for a wide variety of materials, and results indicate that the "lowest temperature to which liquid droplets can be cooled without crystallizing, for nearly all materials lies between 0.75 T_E and 0.85 T_E," [7] where T_E is the equilibrium melt temperature. Tammann, in investigating crystallization in undercooled organic liquids and inorganic glasses, found that "melts which increase rapidly in viscosity during cooling and attain a glassy state, have maxima in their nucleation and growth rates," [6] as shown in Figure 1. Both the nucleation rate and the growth rate are limited at each extreme of undercooling by the existence of metastable zones. "At small degrees of undercooling, there is a metastable zone in which nuclei do not form at any measurable

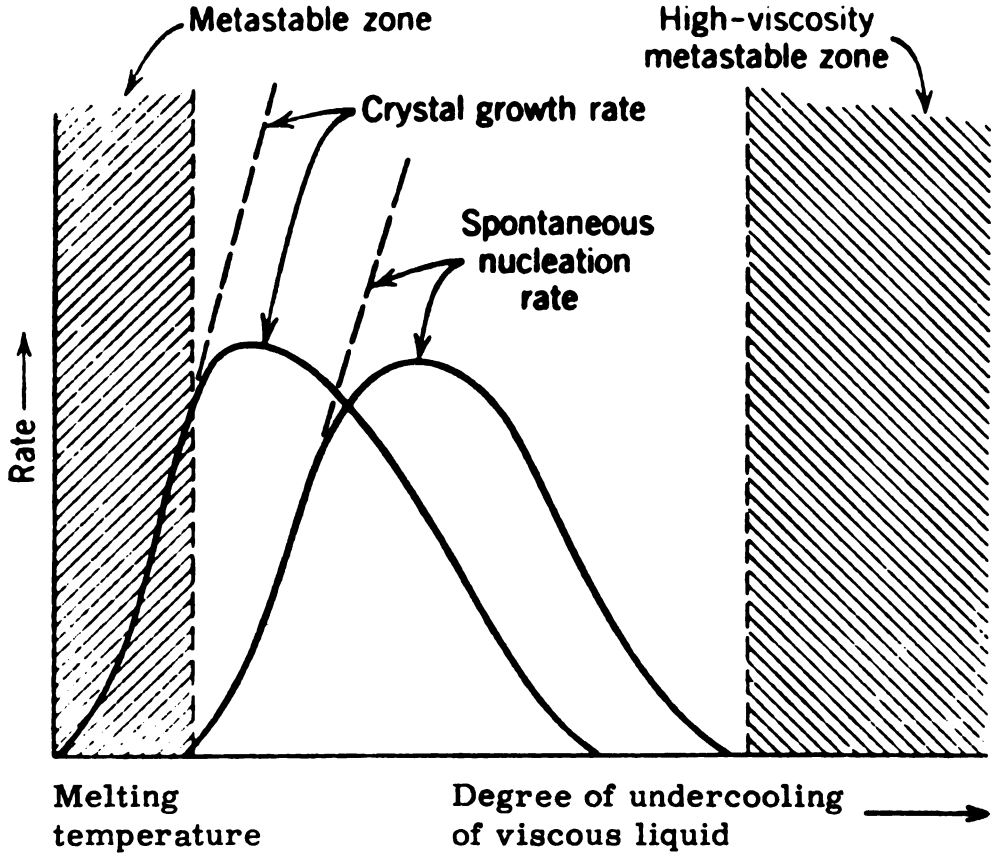

Figure 1. Rates of nucleation and growth for viscous liquids as a function of the degree of undercooling. [6]

rate, but in which crystals,, once nucleated, can grow."[6] At larger degrees of undercooling there is another metastable zone, in which high viscosity prevents crystallization. The maximum in the growth rate curve was found to occur at smaller undercoolings than the maximum in the nucleation rate curve. The implication is that upon cooling, glass-forming melts tend not to crystallize since, owing to the relative positions of the nucleation and growth rate curves, an appreciable number of nuclei are not formed until after the melt has cooled through the region of rapid growth. In this case, crystallization would seem to be limited by the lack of nuclei. And indeed, it has been experimentally verified that many glass-forming materials that fail to crystallize when cooled directly from the melt temperature to a growth temperature, T_g, will crystallize extensively provided that the melt is first cooled to the glassy state and then reheated to T_g. Such observations lend support to the belief that it is not a slow growth rate, but rather a lack of nucleation sites that limits the crystallization of glass-forming melts during cooling. Further support is found in the observation that crystallization in glasses is often found to nucleate from external surfaces, bubbles, and other sources of impurities. Some investigators,[8] however, believe that there are always sufficient nuclei present to initiate crystallization and attribute glass-forming ability to slow growth rates. This dispute has not been satisfactorily resolved, and indeed may persist for some time. The major source of uncertainty is that when crystallization occurs in glasses, it is difficult to determine whether it has occurred through homogeneous nucleation processes, or whether some impurity has nucleated the process.

2.1 Classical Nucleation Theory

Mathematical equations describing the rate of homogeneous nucleation in glass-forming systems have evolved as extensions of classical nucleation theory. Developed to describe condensation in a

supersaturated vapor, classical nucleation theory [9, 10] is built upon the premise that Gibbs free energy is the driving force for condensation. The problem is formulated by considering the effect that droplet condensation has on the free energy of the system. Condensation of a spherical droplet of radius r leads to a change in the system's free energy, ΔF, with

$$\Delta F = \frac{4}{3} \pi r^3 f_v + 4 \pi r^2 f_s \quad , \tag{1}$$

where f_v is the difference in free energy per unit volume between the vapor and the liquid states, and f_s is the free energy per unit surface area (associated with the formation of the vapor-liquid interface). For a supersaturated vapor, f_v is negative and the variation of with r will be as shown in Figure 2. As r increases, ΔF first increases, and then goes through a maximum and decreases. The maximum value of ΔF, denoted ΔF_c, occurs when the droplet radius reaches a critical size r_c, where

$$r_c = \frac{-2 f_s}{f_v} \quad , \tag{2}$$

so that

$$\Delta F_c = \frac{16 \pi f_s^3}{3 f_v^2} \quad . \tag{3}$$

Droplets with radii smaller than r_c are termed "embryos" and tend to evaporate, whereas those with radii larger than r_c are termed "nuclei" and tend to grow. Droplets of critical size are unstable, and may grow or shrink, since either process leads to a decrease in ΔF. The rate of nucleation, I, is given by

$$I = K_1 \exp(-\Delta F_c / kT) \quad , \tag{4}$$

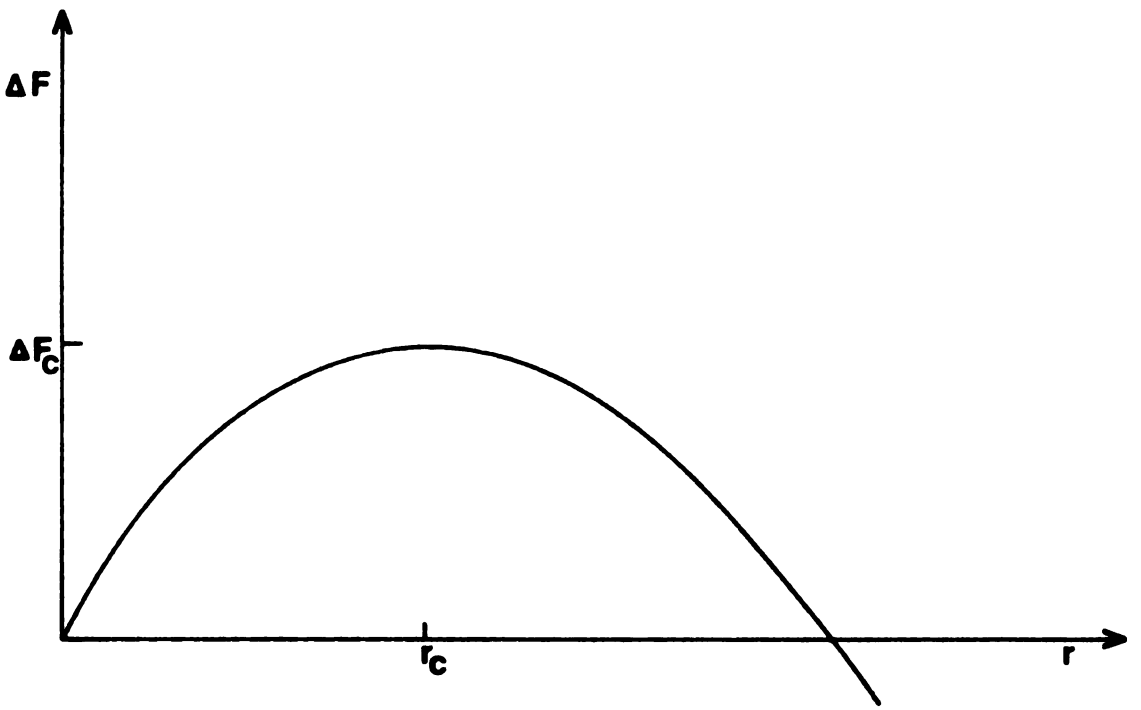

Figure 2. Variation of Gibbs Free Energy with radius for condensation of a spherical droplet in a supersaturated vapor.

where k is Boltzmann's constant, T is absolute temperature, and K_1 is proportional to the probability of a vapor atom's colliding with a critical-size nucleus. Several different expressions have been derived for K_1, which vary depending upon the assumptions made regarding the exact form of the distribution function for embryos in the system. The value of I is dominated by the exponential term, however, so that K_1 is often approximated as the collision frequency of vapor atoms in the system.

The rate of homogeneous nucleation in condensed systems was shown by Becker [10] to be governed by an equation of the form

$$I = K_2 \exp(-\Delta F_c/kT) \quad , \tag{5}$$

provided that K_2 is interpreted as the encounter rate of atoms and ΔF_c is interpreted as the free energy associated with a solid embryo of critical size. In a condensed system, K_2 is given by

$$K_2 = A \exp(-Q/kT) \quad , \tag{6}$$

where A is proportional to the atomic vibrational frequency and Q is the activation energy for diffusion, which in glass-forming systems is often approximated as the activation energy for viscous flow. Upon substituting for K_2, equation 5 can be rewritten as

$$I = A \exp[-(\Delta F_c + Q)/kT] \quad . \tag{7}$$

In glass-forming systems, both ΔF_c and Q are temperature dependent; however, ΔF_c decreases with decreasing temperature, whereas Q increases with decreasing temperature. Thus, the maximum in the nucleation rate, observed experimentally by Tammann for inorganic glass-forming materials, arises in equation 7 from the interplay between ΔF_c and Q with temperature change. Equation 7 may also be used for heterogeneous nucleation, where the presence of impurities effectively lowers the interfacial energy between the nuclei and the

parent phase, provided that a factor is included in equations 1 and 3 to reduce the interfacial energy term f_s.

2.2 Growth Processes

Once formed, nuclei grow at the expense of the parent phase (matrix), securing material of the appropriate composition and arranging this material to fit into the crystalline structure. The rate at which crystalline nuclei grow can be limited by (1) the rate at which material can be transported to the crystal-matrix interface, termed diffusion controlled growth, and/or (2) the rate at which rearrangement at the interface occurs, termed interface controlled growth.

When growth is interface controlled, e.g. in the solidification of a pure melt, a linear dimension of the growing crystal is proportional to time, thus making the growth rate time independent. The growth rate, G, is a function of undercooling, the exact form of which depends upon the assumed mechanism of crystal growth. Essentially three mechanisms for crystal growth have been proposed.

(1) Growth by two-dimensional nucleation[9]-- developed by Gibbs, Becker and Doring, and Frenkel. Crystal growth is assumed to occur through the repeated nucleation and subsequent lateral growth of "island" clusters on close-packed surfaces. Once an island nucleus is formed, it grows laterally by the addition of atoms at the preferential sites, called "steps", which bound the island until the entire crystal surface is covered with another close-packed layer. Further growth cannot occur until another stable island nucleus is formed. Thus, the crystal growth rate is a function of the rate at which island nuclei are formed, and as a result should be proportional to

$$\frac{\exp(-B/\Delta T)}{\eta}$$

where η is the viscosity, ΔT is the degree of undercooling, and B is a constant.

(2) Growth at repeatable steps [9] -- proposed by Frank. This mechanism assumes that crystal growth occurs through the addition of atoms to sites of crystal imperfections, repeatable steps, which are self-perpetuating, e.g. screw dislocations. Since sites are always available for crystals containing these imperfections, close-packed layers are not formed, and the formation of island nuclei, required for the two-dimensional mechanism, is unnecessary. Under these conditions, the crystal growth rate will be proportional to

$$\frac{(\Delta T)^2}{\eta} \quad .$$

(3) Growth without steps [9] -- proposed by Cahn. This mechanism proposes that under certain circumstances (e.g. at high undercoolings) atoms may attach themselves to any position on the crystal interface so that the interface advances uniformly, without steps, at a rate proportional to

$$\frac{\Delta T}{\eta} \quad .$$

In diffusion controlled growth the crystal growth rate is limited by the rate at which material can be transported to and from the growth front. The growth rate, G, is given by

$$G = \alpha D/y \quad , \tag{8}$$

where D is the diffusion coefficient, y is the effective distance over which atoms migrate, and α is a term dependent upon the compositions of the crystal, the matrix, and the interface. In most cases of diffusion controlled growth, a concentration gradient builds up ahead of the growth interface with time, resulting in an increase in the effective distance over which atoms must migrate, so that

$$y = (Dt)^{1/2} \quad , \tag{9}$$

where t is time. Upon substituting for y, equation 8 becomes

$$G = \alpha(D/t)^{1/2} \quad . \tag{10}$$

Under some circumstances, e.g. the growth of a platelet in its own plane or the lengthening of a needle-shaped crystal, crystal growth can proceed without an increase in y. For these cases, a linear dimension of the growing crystal will be proportional to time, and the growth rate will have no time-dependence.

2.3 Crystallization in Glass-Forming Systems

Investigations of crystal growth rates as a function of undercooling in several glass-forming systems suggest that the mechanism of crystal growth may well vary from one system to another. H. R. Swift [11] showed that the growth rates varied linearly with $\Delta T/\eta$ in several soda-lime glasses. A similar dependence of crystal-growth rate on undercooling has since been observed for several simple oxide glasses, [12] e.g. SiO_2, GeO_2, and P_2O_5. In the sodium-silicate system, however, experiments by Scott and Pask [13] indicated that the growth rate varied linearly with $\Delta T^{1.75}/\eta$, and in the lithium-silicate system, experiments by Morley [14] showed that with the appropriate choice of constants the experimental growth rate versus temperature curves could be fitted by either a $\Delta T^{1.75}/\eta$ or an exponential relationship.

The tendency of a glass towards devitrification can often be modified by nucleating agents. Such agents can change the rate of devitrification, the microstructure of the crystalline product, and to some extent, the composition of the crystalline phases. Numerous additives, including noble metals, oxides, fluorides, sulfides, transition-group elements, and halogens, have been found to promote internal crystallization in glasses. The effectiveness of a particular nucleant depends

upon the glass system being nucleated and the concentration in which the nucleant is added. Once a nucleating agent is added to a glass, crystallization is usually brought about by a two-stage heat treatment process in which the glass is first heated at a low temperature to induce nuclei formation, and then at a higher temperature to induce crystal growth.

The mechanism through which a nucleating agent acts varies with both the nucleating agent and the glass system. Some of the reaction paths along which crystallization may proceed in nucleated glasses are shown in Figure 3. [15] Only two of the paths involve crystallization of the nucleant prior to crystallization of the major phase. Each of the four reaction paths is discussed in more detail below.

When devitrification occurs via path 6 - 5, crystallization of the major phase is catalyzed by the crystallization of the nucleating agent. Most of the experimental evidence for this sequence is found with noble metal nucleants. Stookey [16] found that the addition of small amounts of a noble metal to some lithia aluminosilicate glasses produced photosensitive glasses. Photonucleation resulted in the growth of metallic crystals which served as nucleation sites for the crystallization of lithium metasilicate. This reaction path has not been commonly observed for other nucleating agents.

Crystallization occurring along path 2 - 3 has been observed and is the source of much debate. Glasses following this crystallization sequence exhibit glass-in-glass phase separation prior to crystallization of the major phase. Amorphous phase separation describes the process whereby a glass separates into two amorphous phases, with droplets of one phase dispersed in a matrix of the other phase. This process is caused by the immiscibility of the two phases, and hence is dependent upon composition and temperature. Only certain glass systems undergo phase separation, and then only over a specific range of composition and temperature. Nucleating agents have been found to influence the ability of a glass to phase separate [12] --

AMORPHOUS PHASE
SEPARATION

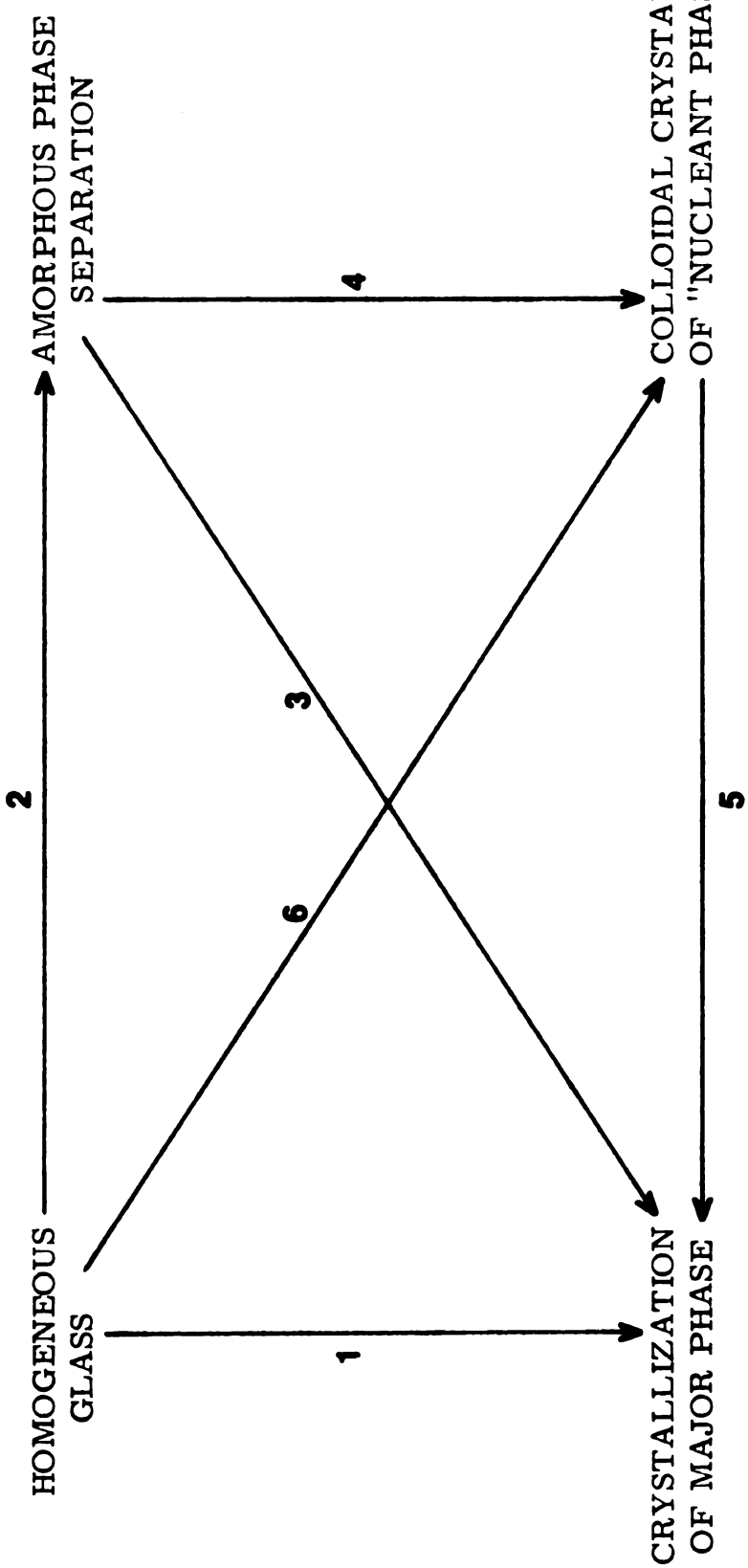

Figure 3. Reaction paths between the initial glass and the final glass-ceramic.[15]

sometimes suppressing phase separation, e.g. Al_2O_3 in sodium borosilicate glasses, and sometimes enhancing phase separation, e.g. P_2O_5 in sodium silicate glass. Whether phase separation is always a precursor to crystallization has been debated. It seems likely that phase separation may often be associated with, but not required for, subsequent crystallization.

Glasses crystallizing along path 2 - 4 - 5 undergo phase separation followed by crystallization of the nucleating agent, which in turn is followed by crystallization of the glass. Such a sequence was observed for a magnesium aluminosilicate glass containing titania,[16] where phase separation was followed first by crystallization of magnesium titanate and then by crystallization of the major phase. Again, no cause-effect relationship has been established between phase separation and the subsequent crystallization of the major phase. Results of one study suggested "that the colloidal crystals of the nucleant phase which occur after the amorphous phase separation and before crystallization of the major phase are not necessarily an integral part of the nucleation of the major phase". [17]

Reaction path 1, in which a homogeneous glass crystallizes directly into its major phases without phase separation or crystallization of a nucleant phase, has not been observed as a common occurrence, although such a course was followed by TiO_2 nucleated lithia aluminosilicate glass, according to Barry et al.. [18, 19]

CHAPTER III
THE LEAD SILICATE SYSTEM

There are two naturally occurring lead silicate compounds - the minerals Alamosite ($PbO \cdot SiO_2$) and Barysilite ($3PbO \cdot 2SiO_2$). In addition, several lead silicate compounds have been synthesized by the devitrification or by the sintering of PbO and SiO_2. For many years the accepted phase diagram of the lead silicate system was that of Geller, Creamer, and Bunting,[20] which is shown in Figure 4. Three stable lead silicate compounds with $PbO:SiO_2$ ratios of 4:1, 2:1, and 1:1 are shown. The $4PbO \cdot SiO_2$ compound has three polymorphic modifications, and the $PbO \cdot SiO_2$ compound corresponds to the mineral Alamosite. The work of other investigators, however, has indicated the existence of additional compounds, some of which may be metastable. Since devitrification in the lead silicate system may be complicated by the existence of metastable phases, this chapter will first review the various investigations that have been made of phase relations in the lead silicate system. Then, the results of previous kinetic studies of lead silicate compounds will be presented.

3.1 Compound Formation

In 1909 Cooper, Shaw, and Loomis [21] investigated the thermal properties of the lead silicate system. Heating curves were determined for a number of crystalline samples, which had been prepared from slowly cooled melts whose compositions ranged from 43 to 100 mole percent PbO. Melting points of the various compositions were determined from breaks in their heating curves and used to construct melting point curves. On the basis of the melting point data, the orthosilicate and metasilicate compositions, $2PbO \cdot SiO_2$ and $PbO \cdot SiO_2$

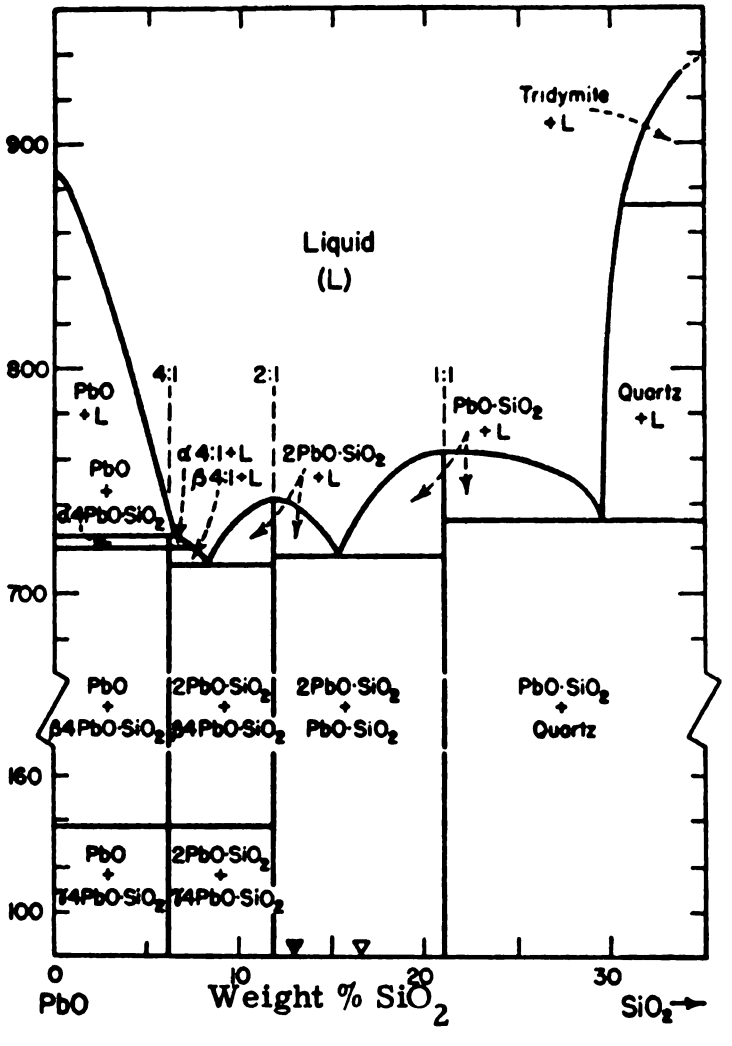

Figure 4. Phase diagram of the lead silicate system by Geller et al.[20] The actual composition of the 70-30 base glass studied in this investigation is indicated by the solid triangle along the base line, that of the 60-40 base glass with the open triangle.

respectively, were established as lead silicate compounds. Well defined maxima in the curve corresponded to the melting points of these two compounds. Two eutectic points were found over the composition range studied: one occurred between the lead oxide and the orthosilicate compositions, while the other occurred between the orthosilicate and the metasilicate compositions.

The following year Hilpert and Nacken [22] reported that their work indicated the existence of the orthosilicate and metasilicate compounds and the possible existence of compounds with compositions $3PbO \cdot SiO_2$ and $3PbO \cdot 2SiO_2$.

Investigations of the lead silicate system begun by Cooper, Shaw, and Loomis [21] were continued by Cooper, Kraus, and Klein [23] and extended to cover optical, as well as thermal, properties. Their study included observations of both natural minerals Alamosite and Barysilite and synthetic lead silicate crystals prepared by the slow cooling of lead oxide-silica melts. Results of optical and thermal analyses led the authors to conclude that the compositions $PbO \cdot SiO_2$, $2PbO \cdot SiO_2$, and $3PbO \cdot 2SiO_2$ existed as compounds in the lead silicate system. Properties of the $PbO \cdot SiO_2$ and the $3PbO \cdot 2SiO_2$ compounds prepared in the laboratory were found to correspond to those of naturally occurring Alamosite and Barysilite. The existence of a compound with the composition $3PbO \cdot SiO_2$ was deemed probable on the basis of its sharp melting point and its somewhat anomalous optical characteristics.

In 1931 Krakau and Vakhromeev [24] reported results of their thermal and optical investigations of the lead silicate system, and in basic agreement with previous studies, they concluded that four compounds existed: $3PbO \cdot SiO_2$, $2PbO \cdot SiO_2$, $3PbO \cdot 2SiO_2$, and $PbO \cdot SiO_2$. In addition, a polymorphic transformation at 620^0C was found in the orthosilicate compound.

A few years later Geller et al. [20] conducted their investigation which indicated the existence of three stable compounds in the lead

silicate system, namely $4PbO \cdot SiO_2$, $2PbO \cdot SiO_2$, and $PbO \cdot SiO_2$. Identification of the compounds with compositions $2PbO \cdot SiO_2$ and $PbO \cdot SiO_2$ was in close agreement with earlier reports, as were the values determined for their melting points. The $4PbO \cdot SiO_2$ compound, however, had not previously been reported. More important was the omission of compounds with compositions of $3PbO \cdot SiO_2$ and $3PbO \cdot 2SiO_2$ from the phase diagram presented by Geller et al. . Attempts by Geller et al. to synthesize either compound were unsuccessful. Mixtures containing 20 mole percent SiO_2 crystallized as a single phase, which formed PbO and glass upon heating to 725°C - 735°C. The authors suggested that their $4PbO \cdot SiO_2$ compound was the $3PbO \cdot SiO_2$ compound reported by Krakau and Vakhrameev. Mixtures of the $3PbO \cdot 2SiO_2$ composition were found to crystallize into a combination of orthosilicate and metasilicate after a heat treatment of 20 hours at 705°C; while "specimens quenched after holding 3 hours or less at the same temperature consisted almost wholly of a phase resembling Barysilite in color and index of refraction, but which was either all glass or glass containing extremely minute crystals." [20]

The existence of the compounds $2PbO \cdot SiO_2$ and $PbO \cdot SiO_2$ was verified with x-ray diffraction in 1935 by Valenkov and Porai-Koshits.[24] They concluded that the compounds $3PbO \cdot SiO_2$ and $3PbO \cdot 2SiO_2$, as well as the $4PbO \cdot SiO_2$ compound reported by Geller et al.,[20] did not exist as stable phases in the lead silicate system. The $4PbO \cdot SiO_2$ composition yielded mixtures of βPbO and $2PbO \cdot SiO_2$.[25]

In 1939 an x-ray diffraction investigation was conducted by McMurdie and Bunting [25] to verify the existence of the compounds that had been reported earlier by Geller et al. .[20] Their results indicated that the compounds $4PbO \cdot SiO_2$, $2PbO \cdot SiO_2$, and $PbO \cdot SiO_2$ did exist in the lead silicate system. Further, they reported that the diffraction patterns obtained from the $4PbO \cdot SiO_2$ compound could not have arisen from a mixture of βPbO and $2PbO \cdot SiO_2$, as had been suggested by Valenkov and Porai-Koshits.[24]

The existence of $2PbO \cdot SiO_2$ and $PbO \cdot SiO_2$ was verified again in 1956 by Milent'eva and Solov'eva [24] with thermographic and microscopic analyses. In 1960 Argyle and Hummel [26] made an x-ray and dilatometric study of synthetic lead silicate compounds. They, too, were able to verify the existence of the $2PbO \cdot SiO_2$ and $PbO \cdot SiO_2$ compounds. No polymorphic transformation was reported for the $2PbO \cdot SiO_2$ compound in as much as this phase exhibited no discontinuities in the thermal-expansion curve. This result was in agreement with the findings of Geller and co-workers. Argyle and Hummel also verified the existence of the $4PbO \cdot SiO_2$ compound, including the transformation of γ-$4PbO \cdot SiO_2$ to β-$4PbO \cdot SiO_2$. The β to α inversion was not observed; the authors felt, however, that this inversion would have been difficult to detect by thermal-expansion methods. Attempts to prepare the $3PbO \cdot SiO_2$ and the $3PbO \cdot 2SiO_2$ compounds by high-temperature sintering and devitrification techniques failed, as mixtures of $4PbO \cdot SiO_2$ and $2PbO \cdot SiO_2$ were obtained for the $3PbO \cdot SiO_2$ composition, and mixtures of $2PbO \cdot SiO_2$ and $PbO \cdot SiO_2$ were obtained for the $3PbO \cdot 2SiO_2$ composition. These investigators concluded that these two compositions probably did not exist under normal conditions of temperature and pressure.

Work on the lead silicate system was taken up again a few years later by Berezkina and Chizhikov [24] with an x-ray diffraction study aimed at determining the compositions of the compounds present in the system. Crystalline samples were obtained by devitrification of melts of lead oxide and silica. Their work confirmed the existence of $4PbO \cdot SiO_2$, $2PbO \cdot SiO_2$, and $PbO \cdot SiO_2$. Two polymorphic modifications of lead orthosilicate were found. Furthermore, $3PbO \cdot 2SiO_2$ was reported to occur as a distinct compound which existed, however, only over a narrow temperature range near the melting point. At lower temperatures, the compound became unstable and decomposed into a mixture of $2PbO \cdot SiO_2$ and $PbO \cdot SiO_2$. The $3PbO \cdot SiO_2$ composition was found to crystallize as a mixture of $4PbO \cdot SiO_2$ and $2PbO \cdot SiO_2$.

Smirnova,[27,28,29] in the late 1960's, made several studies of crystallization in lead silicate glasses utilizing infrared spectroscopy, electron microscopy, and x-ray diffraction techniques. Results indicated that there were at least two polymorphic modifications for both the $2PbO \cdot SiO_2$ and the $PbO \cdot SiO_2$ compounds. The transition for the orthosilicate occurred between 450°C and 620°C. The modifications for the $PbO \cdot SiO_2$ compound arose from differences between surface crystals and internal crystals.

In 1967 Pavlushkin and Lisovskaya [1] reported that crystallization of lead silicate glass of composition close to 60 mole percent PbO resulted in mostly $2PbO \cdot SiO_2$. A year later they reported [2] that crystallization of a glass containing 60 mole percent PbO at 600°C produced crystals of the following compounds: $2PbO \cdot SiO_2$, $4PbO \cdot SiO_2$, and $3PbO \cdot 2SiO_2$. A more recent study,[3] published in 1971 concluded that the same glass crystallized into a combination of $2PbO \cdot SiO_2$ and $4PbO \cdot SiO_2$ when heat treated at temperatures of 450°C and 550°C.

In the various studies made on the lead silicate system, only the existence of the compounds $2PbO \cdot SiO_2$ and $PbO \cdot SiO_2$ was agreed upon. Controversy surrounded the existence of compounds with compositions of $4PbO \cdot SiO_2$, $3PbO \cdot SiO_2$, and $3PbO \cdot 2SiO_2$. In addition there was no agreement as to the existence of polymorphic modifications for the $2PbO \cdot SiO_2$ and $PbO \cdot SiO_2$ compounds. In an effort to resolve this controversy, Ott and McLaren [30] conducted a DTA and x-ray diffraction investigation of the system. The resulting phase diagram appeared in 1970, and is given in Figure 5. The region above 700°C was based on the phase diagram of Geller et al..[20] The authors cautioned, however, that since crystallization occurred very slowly, their proposed phase diagram might not be a true equilibrium diagram due to the possible inclusion of metastable phases. X-ray diffraction analysis indicated the existence of compounds $4PbO \cdot SiO_2$, $3PbO \cdot SiO_2$, $2PbO \cdot SiO_2$, $3PbO \cdot 2SiO_2$, and $PbO \cdot SiO_2$. The three modifications of $4PbO \cdot SiO_2$, reported

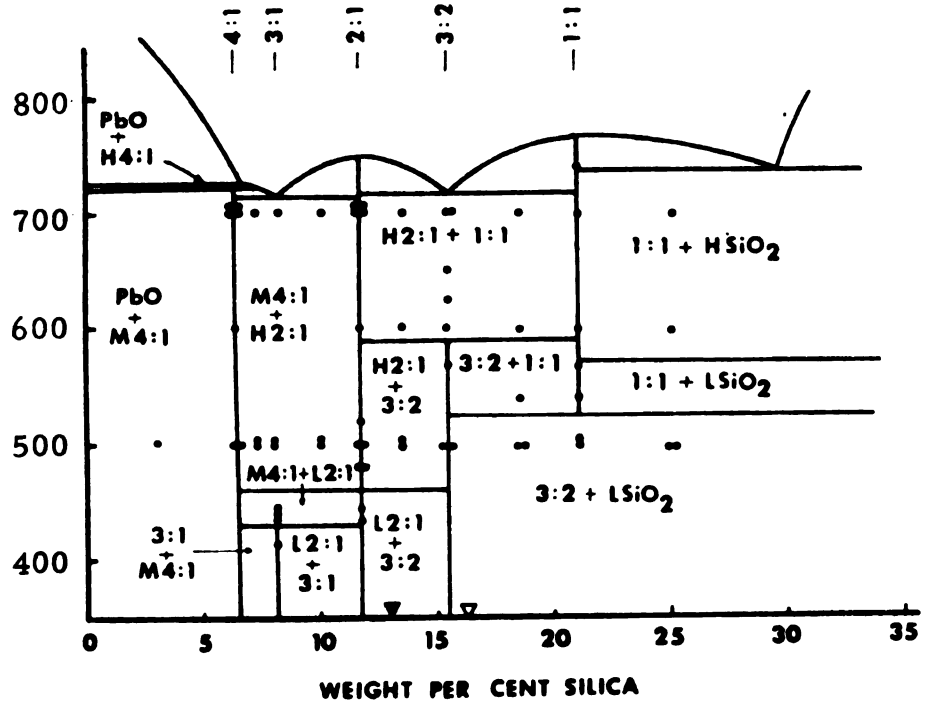

Figure 5. Phase diagram of the lead silicate system by Ott and McLaren.[30] The solid triangle along the base line indicates the actual composition of the 70-30 base glass studied in this investigation, the open triangle the actual composition of the 60-40 base glass.

by Geller et al.,[20] were confirmed, as were the two modifications of $2PbO \cdot SiO_2$, as reported earlier by Krakau and Vakhrameev,[24] Berezkina and Chizhidov,[24] and Smirnova et al.[27,28,29] The $3PbO \cdot SiO_2$ and $3PbO \cdot 2SiO_2$ compounds were found only at low temperatures and were determined to be unstable above 430°C and 585°C respectively. In addition, Ott and McLaren found that the $PbO \cdot SiO_2$ compound was unstable below 525°C, decomposing into a mixture of $3PbO \cdot 2SiO_2$ and SiO_2. Ott and McLaren's work somewhat clarified the controversy surrounding the lead silicate system.

A study of compound formation in the lead silicate system by Smart and Glasser [31] also helped to resolve some of the apparent contradictions of earlier investigations. The resulting phase diagram, which is presented in Figure 6, is quite similar to that of Geller et al..[20] One major difference between the two diagrams is the inclusion by Smart and Glasser of a stability field for the $3PbO \cdot SiO_2$ compound. Another difference was the inclusion of $5PbO \cdot 8SiO_2$ as a possible stable compound. In all, fifteen lead silicate compounds were prepared by Smart and Glasser, including two modifications of the $3PbO \cdot 2SiO_2$ compound. Many of these compounds, however, were determined to be metastable phases and hence were excluded from the proposed phase diagram. The authors suggested that the metastable phases arise as intermediate crystallization products, which eventually convert into stable crystalline phases.

3.2 Rate of Crystallization

The crystallization velocity of lead silicates has been studied by Hilpert and Nacken [22] and by Rita and Bergeron.[32] In 1910, Hilpert and Nacken [22] reported results of their study on the crystallization of $2PbO \cdot SiO_2$ and $PbO \cdot SiO_2$. Both compounds reached maxima in their growth rates at approximately 690°C. The maximum growth rate of 120 mm/hr observed for the orthosilicate compound, $2PbO \cdot SiO_2$, was substantially higher than the 20 mm/hr maximum observed for the

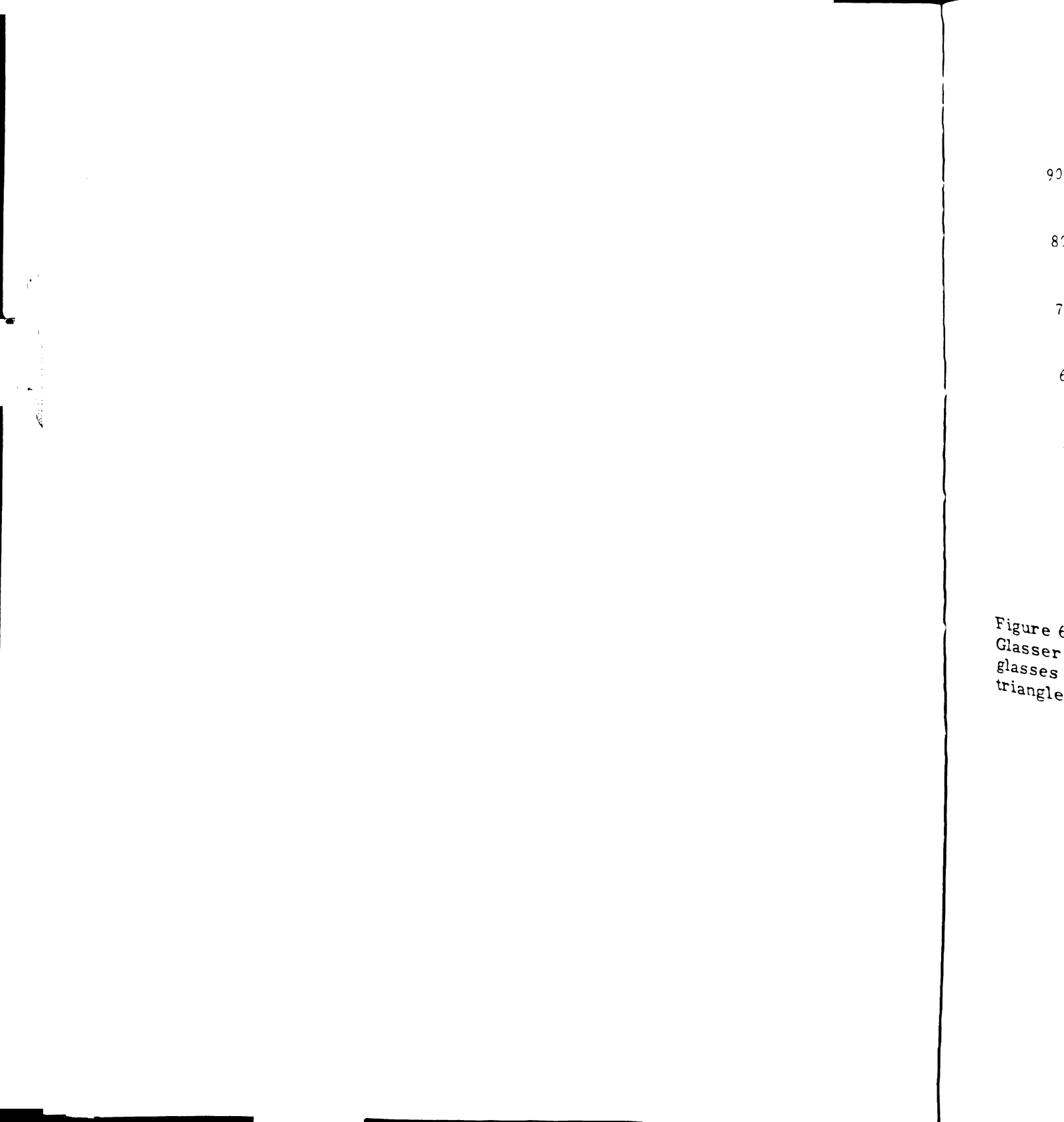

Figure 6
Glasser
glasses
triangle

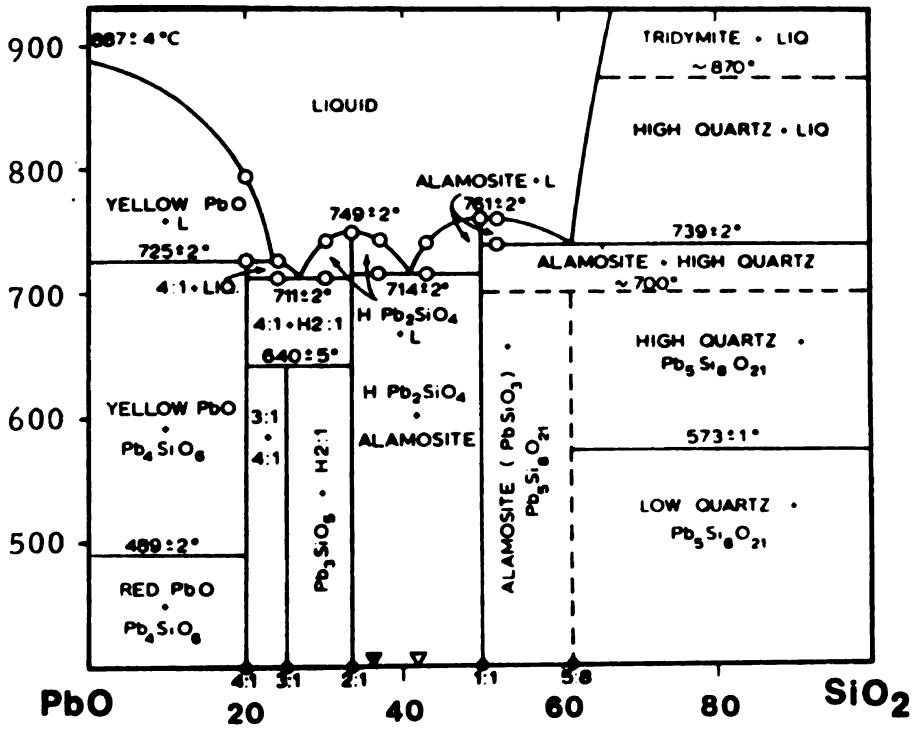

Figure 6. Phase diagram of the lead silicate system by Smart and Glasser.[31] The actual compositions of the 70-30 and 60-40 base glasses studied in this investigation are indicated by solid and open triangles, respectively, that lie along the base line.

metasilicate compound, $PbO \cdot SiO_2$. Both compounds also exhibited regions of spontaneous crystallization -- ranging from 630°C to 400°C for $2PbO \cdot SiO_2$ and from 670°C to 470°C for $PbO \cdot SiO_2$ -- over which rapid formation of nuclei interfered with growth rate measurements. Below this region the growth rates of both compounds dropped off significantly. For the orthosilicate compound the crystal growth rate was reduced to about 1 mm/hr, and that of the metasilicate compound was too small to measure.

Rita and Bergeron [32] published results of their study of the crystallization of $2PbO \cdot SiO_2$ in 1976. Crystal growth was measured over the temperature range of 500°C to 740°C with a maximum growth rate of 28 μm/sec occurring at approximately 690°C. According to the authors, the growth rate data did not appear to fit any of the standard crystal growth models.

CHAPTER IV
EXPERIMENTAL PROCEDURE

4.1 Glass Preparation

All glasses in this study were prepared from analytical reagent grade PbO and 30 μm Min-U-Sil, a high-purity form of silica. Phosphorus pentoxide was added in the form of ammonium dihydrogen phosphate. Two nominal compositions of base glasses were prepared -- one containing 70 mole percent PbO and 30 mole percent SiO_2, and the other containing 60 mole percent PbO and 40 mole percent SiO_2, hereafter referred to as 70-30 and 60-40 respectively. Ammonium dihydrogen phosphate was added to the 60-40 base glass to give glasses with 0.1 and 0.5 mole percent P_2O_5, designated as 60-40-0.1 and 60-40-0.5 respectively, and to the 70-30 base glass to give glasses with 0.5 and 1.0 mole percent P_2O_5, designated as 70-30-0.5 and 70-30-1.0.

After careful consideration, 900°C was selected as the melting temperature for glass formation. This temperature was considered high enough to insure complete melting of the batch materials, since it is above the melting points of both PbO and the glasses being formed, and yet low enough to avoid drastically altering the final composition of the glasses through excessive volatilization.

The high lead oxide content of the glasses made the melting procedure a bit difficult. The melts were extremely corrosive, especially at the high melt temperature used, and readily attacked the crucibles in which they were being melted. Several batches were lost when the melts dissolved the crucibles. Alumina, fused silica, and Vycor crucibles were tried with varying degrees of success. Alumina crucibles held up the best. The thick walled Norton alumina crucibles (70318) were capable of holding the melt up to 4 or 5 hours. The Vycor

crucibles usually held melts for 1 or 2 hours, and the fused silica crucibles dissolved rapidly, usually in less than 1 hour. The alumina crucibles were, in spite of their superior performance, not ultimately used for glass formation since any alumina dissolved from the crucible by the melt would go into solution and remain as an impurity in the glass. Since the melts were so corrosive, there was a strong possibility that the amount of alumina picked up by the glass during the melting operation would be even larger than the amount of P_2O_5 being added as a nucleating agent. This was later confirmed by microprobe analysis which showed that glasses melted in alumina crucibles contained as much as 2 percent aluminum. Vycor, on the other hand, is made from sodium borosilicate glass from which the sodium borate phase has been leached out, leaving behind a network of 96% SiO_2. Batch material melted in Vycor crucibles would probably pick up some additional SiO_2; however, no significant amount of impurity would be added to the glasses being formed. For this reason, Vycor crucibles were selected for all batch melting.

The corrosive nature of the melts made it necessary to keep the time required for adding batch material to the crucible as short as possible. Therefore, all glasses were made in a Lindberg Hevi-Duty furnace which was capable of reaching the melt temperature very rapidly, usually within 30 minutes. During this time, frequent additions of batch material were made to the crucible so that when the furnace reached 900°C, all batch material was added and molten. The melt was then held at 900°C for 1 hour. This procedure worked reasonably well, and only occasionally were melts lost due to crucible failure. The complete procedure followed in making the glass samples is listed below.

1. PbO and SiO_2 were weighed out and thoroughly mixed. Glasses were made in 150 gm batches.
2. Vycor crucibles were placed in the furnace and the batch materials were added as the furnace was heating.

3. Melts were held at 900°C for 1 hour.
4. At the end of 1 hour, the melts were quenched in water, yielding fine, glassy pellets of the base compositions.
5. The glass pellets were crushed and sifted through a 400 mesh sieve.
6. The sifted glass powder was weighed out in 150 gm batches.
7. Ammonium dihydrogen phosphate was weighed out and added to the powdered base glass to form the P_2O_5 nucleated glasses.
8. All batches were remelted in new crucibles according to steps 2 and 3.
9. Finally, the melts were quenched between steel plates, producing glass plates, approximately 1/8 in. thick.

4.2 Devitrification of Glasses

The crystallization of each glass was studied at temperatures of 400°C, 450°C, 500°C, and 550°C. Samples were placed in graphite crucibles and inserted into thermally equilibrated furnaces. The heat treatment time was measured from the time of the sample's insertion to the time of its removal from the furnace. During heat treatment, the furnace temperature was monitored with a calibrated thermocouple to determine: (1) the length of time required for the furnace to re-equilibrate after insertion of the sample, and (2) the maximum fluctuation in temperature that occurred during the heat treatment. The furnace usually regained crystallization temperature within 3 to 4 minutes. Heat treatment times ranged from a few hours for crystallization at 450°C to several days for crystallization at 400°C. For both of these cases, the time required for the furnace to regain equilibrium after sample insertion was considered negligible with respect to the long heat treatment times involved. Crystallization heat treatment times at 500°C ranged from 10 minutes to 140 minutes, and the furnace recovery time was again neglected. For crystallization at 550°C, however, heat treatment times were so short, ranging from 3 to 10 minutes for the 70-30-1.0 composition, that a way had to be

devised for inserting the glass samples without lowering the temperature of the furnace. This was accomplished by using a furnace with a small front window and equilibrating it with the window open. The open front window had no noticeable effect on the stability of the furnace temperature. Glass samples to be heat treated were placed in a small basket that had been formed at the end of a long metal rod. With the basket, it was easy to insert and remove the sample through the window without disrupting the equilibrium of the furnace. The maximum temperature fluctuation observed during heat treatment at any temperature, after the furnace re-equilibrated, was less than $8^{0}C$.

4.3 Methods of Observation and Analysis

The size and morphology of crystals in devitrified samples were studied by light microscopy, utilizing both the reflected and transmitted light modes. Thin sections of samples were prepared for study under transmitted light, while polished faces, which had been lightly etched with 1% HNO_3, were used for reflected light microscopy. The diameters of the crystals in each sample were measured from micrographs taken at random intervals over the sample. Using this data, histograms showing the size distribution of the crystals in each sample were constructed. Then the mean radius, and standard deviation, of each crystal population were calculated and plotted versus growth time. The crystal growth rate was determined as the slope of the best fit straight line through these points. Data points were subjected to t-analysis and were rejected only if they lay outside of 95% confidence limits.

Transmission electron microscopy was used to examine the ultrastructure of both the quenched and the devitrified glasses. Samples were studied by replication and by direct observation of thin sections. The thin sections were obtained by microtoming samples on a Porter-Bluhm II microtome, equipped with a diamond knife.

Figure 7 shows the instrument set-up. The sample is drawn over the stationary knife edge at a constant, predetermined velocity. After each pass, the microtome automatically retracts the sample, swings it back up to the top of the cycle, and advances the sample a set distance, which becomes the thickness of the section cut on the next pass. Cut sections float off the knife edge and into the boat where they are later picked up onto grids. The samples were rather difficult to section, and often only shattered fragments of glass were obtained. When intact thin sections were obtained, however, they were uniformly thin and of much higher quality than thin foils prepared by other methods, e.g. chemical or mechanical thinning.

Samples were also studied by the replication method. Replicas were made of (1) freshly fractured, (2) freshly fractured and then etched, and (3) polished and then etched surfaces. Usually, however, either fractured surfaces or fractured and then etched surfaces were used as these seemed to produce the most consistent results. Most replicas were prepared by the two-stage process in which the surface features of the sample are impressed into replicating tape, which is subsequently shadowed with a heavy metal and then backed with a layer of carbon. The plastic tape is then dissolved, leaving a metal-shadowed carbon replica of the surface. Some difficulty was encountered in dissolving the tape from the replica. Removing the plastic by placing the plastic-backed replicas on grids which are then either (1) placed on filter paper which is kept saturated with acetone until the plastic is dissolved or (2) placed on fine mesh screens in containers which are kept filled with acetone to the level of the screen until the plastic is dissolved, often resulted in badly torn, sometimes completely destroyed, replicas due to the swelling of the tape which occurred during the dissolving process. An alternative method, [33, 34] in which the replicas are washed in an atmosphere of refluxing acetone, was found to produce cleaner, virtually intact, replicas and was adopted as the normal procedure for removing the plastic backing.

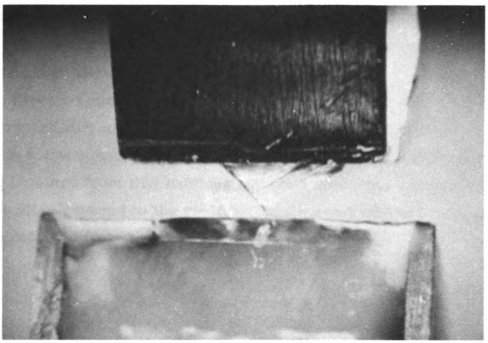

Figure 7. Microtome set-up for sectioning glass.

Occasionally single-stage metal-shadowed carbon replicas were made. The heavy-metal shadowing and subsequent carbon backing were deposited directly onto the glass surface, and then the replica was removed by scoring the deposited film and floating pieces off in a solution of nitric acid.

Electron and x-ray diffraction techniques were used to check for crystallinity and to determine d-spacings for the crystalline compounds formed during devitrification. Electron diffraction patterns were obtained from thin sections and from extracted crystal fragments which often adhered to the replicas, while x-ray diffraction spectra were obtained from powdered, devitrified samples.

CHAPTER V
RESULTS AND DISCUSSION

5. 1 Crystallization Products

For all compositions studied, the melting procedure yielded clear, yellow glasses. Chemical analysis indicated that the glasses picked up silica during the melting operation. The 70-30 base composition produced a glass containing 64 mole percent PbO and the 60-40 base composition produced a glass containing 59 mole percent PbO. The actual compositions of both glasses are shown on the phase diagrams in Figures 4, 5, and 6. The 70-30 glass is close to the $3PbO\text{-}2SiO_2$ eutectic, as shown in Figure 5, and is of the same composition that was studied by Pavlushkin et al.[1,2,3] Figures 4 and 6 indicate that the crystallization products in both the 70-30 and the 60-40 glasses would be the same, namely $2PbO\cdot SiO_2$ and $PbO\cdot SiO_2$. However, Figure 5 indicates that over the temperature range 400°C to 550°C, the crystallization products of the 70-30 glass would be $3PbO\cdot 2SiO_2$ and $2PbO\cdot SiO_2$, and those of the 60-40 glass would be $3PbO\cdot 2SiO_2$ and $PbO\cdot SiO_2$ or L-SiO_2.

X-ray diffraction spectra for the 70-30 composition, after prolonged heat treatment at 400°C, 450°C, 500°C, and 550°C are shown in Figure 8. Curve (a), corresponding to a heat treatment of 7 days at 400°C, consists of only one broad peak, located between $25^0 < 2\theta < 33^0$ indicating that crystallization has not proceeded very far. Upon comparing the other three spectra for heat treatments at 450°C, 500°C, and 550°C, two trends can be seen.

(1) The peaks marked with solid arrows on curve (d) constitute the major peaks for specimens heat treated at 550°C and 500°C and are also found in the spectra of specimens devitrified at 450°C. These

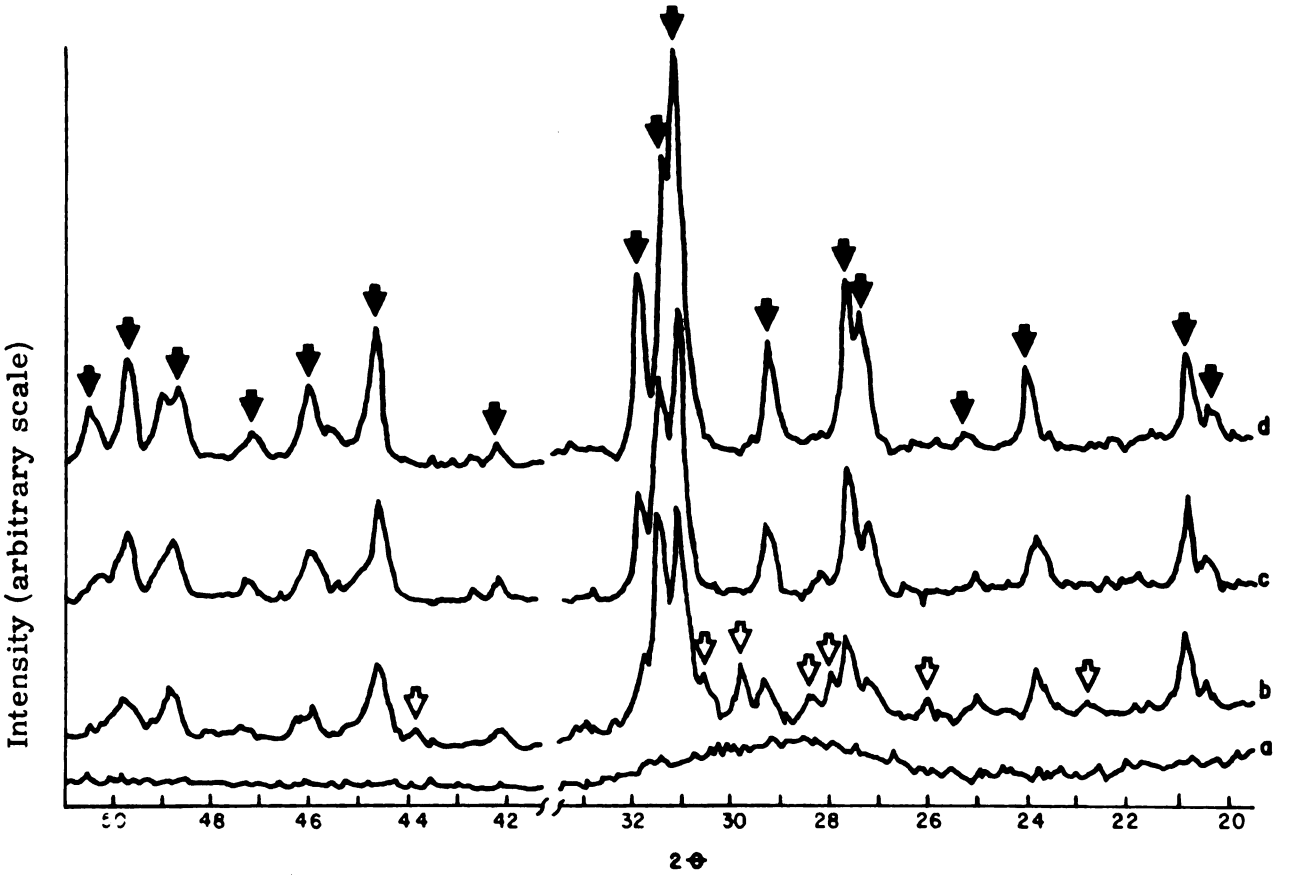

Figure 8. X-ray diffraction spectra of 70-30 glass devitrified for (a) 7 days at 400°C, (b) 6 days at 450°C, (c) 3 days at 500°C, and (d) 3 days at 550°C. The solid arrows on curve (d) indicate the diffraction peaks attributed to the major crystalline phase. The open arrows on curve (b) indicate the diffraction peaks of the low temperature, secondary phase.

peaks occur with approximately the same relative intensities in all three spectra and show a gradual sharpening and intensification with increasing crystallization temperature. These peaks are probably associated with the major crystalline phase, which apparently is stable over the temperature range 450°C to 550°C.

(2) The peaks marked with open arrows on curve (b) decrease in intensity as the heat treatment temperature increases, disappearing completely at 500°C. X-ray spectra of glasses heat treated for shorter periods of time at 500°C and 550°C also did not reveal these peaks. These peaks most likely belong to a low-temperature, secondary phase which becomes unstable about 500°C.

The d-spacings and relative intensities for the major crystalline phase are given in Table 1, while those of the low-temperature, secondary phase are presented in Table 2. The major crystalline phase can be identified on the basis of its x-ray diffraction spectra as a polymorph of $3PbO{\cdot}2SiO_2$. Although there are some inconsistencies in the published x-ray diffraction data of several lead silicate compounds, there is good agreement by three investigators [30,31,35] on the spectra of this $3PbO{\cdot}2SiO_2$ modification. Both Smart and Glasser [31] and Billhardt [35] identified a low-temperature modification of Barysilite which formed readily upon devitrification of lead silicate glasses containing 60 mole percent PbO. The x-ray diffraction data obtained by Smart and Glasser [31] for this compound, while not given, was reported to agree with that of Billhardt.[35] The x-ray data of Ott and McLaren,[30] for their $3PbO{\cdot}2SiO_2$ compound, was also in agreement with that of Billhardt.[35] In all three studies, the $3PbO{\cdot}2SiO_2$ modification was obtained only through devitrification and was found to be unstable at temperatures above 585°C - 650°C. Attempts by Smart and Glasser [31] and by Ott and McLaren [30] to synthesize this compound from sintered mixtures of other crystalline phases failed, leading Ott and McLaren [30] to question the compound's existence as an equilibrium phase and causing Smart and Glasser [31] to conclude that

Table 1. The d-spacings and relative intensities of the x-ray spectra for the major crystalline phase.

d(Å)	I/I_0						
	550°C				500°C		450°C
	70-30	70-30-1.0	60-40	60-40-0.5	70-30	60-40	70-30
4.37	9	14	14	13	11	13	12
4.29	21	30	33	30	32	33	33
3.72	18	20	25	18	18	21	24
3.53	6	-	-	9	5	-	10
3.27	35	34	35	40	25	24	21
3.23	42	43	64	54	43	60	43
3.06	28	28	23	32	23	28	21
2.87	100	100	100	100	100	100	100
2.86	72	85	86	84	79	92	100
2.81	43	37	64	42	36	43	36
2.14	6	6	-	7	7	11	10
2.03	35	35	30	32	33	32	36
1.97	20	18	18	17	18	19	17
1.93	7	9	9	9	7	13	-
1.87	18	24	25	22	21	24	26
1.83	26	35	21	32	23	24	21
1.81	11	-	10	-	7	8	-

Table 2. The d-spacings and relative intensities of the x-ray spectra for the low temperature phase in devitrified 70-30 glass.

d(Å)	I/I_0
3.90	33
3.41	50
3.18	83
3.14	50
2.99	100
2.93	67
2.05	25

the compound was metastable. Although there is some doubt as to whether or not this compound is stable in the strict thermodynamic sense, these investigators recognized that below 585°C - 650°C this modification of $3PbO \cdot 2SiO_2$ is a very persistent phase. In fact, Smart and Glasser [31] found that this phase only partially decomposed after being heated at 580°C for 21 days. In the course of this study, decomposition of the major phase was never observed.

The d-spacings and relative intensities attributed to the low-temperature, secondary phase in devitrified 70-30 glass agree quite well with those listed by Ott and McLaren [30] for a low-temperature polymorph of $2PbO \cdot SiO_2$. In addition, the presence of this phase in the x-ray spectra for glass devitrified only at 450°C is in accord with the polymorphic transition reported by Ott and McLaren [30] at 460°C ± 15°C for $2PbO \cdot SiO_2$. Smart and Glasser [31] and Billhardt [36] also observed the low $2PbO \cdot SiO_2$ phase. Three metastable and one stable polymorphs of $2PbO \cdot SiO_2$ were reported by Smart and Glasser,[31] designated L, M, M', and H respectively. The interphase relationships were seen as:

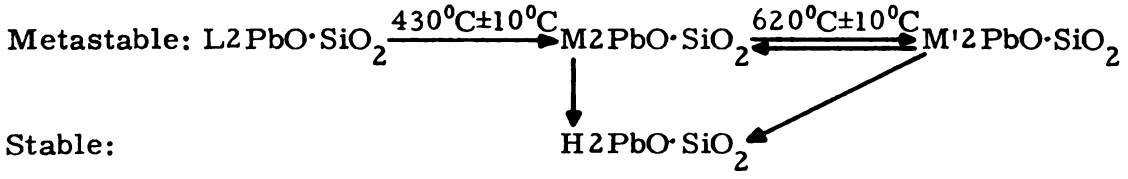

Although x-ray data was not given by Smart and Glasser [31] for $L2PbO \cdot SiO_2$, their $L2PbO \cdot SiO_2$ phase was identified with the low-$2PbO \cdot SiO_2$ phase obtained by Ott and McLaren.[30] Thus, the low-temperature, secondary phase present at 450°C in devitrified 70-30 glass is probably low-$2PbO \cdot SiO_2$. The absence of any $2PbO \cdot SiO_2$ compound (e.g. M, M', or H) at temperatures above 450°C is puzzling since the 72 hour heat treatments used in this study at 500°C and 550°C to devitrify samples for x-ray analysis are comparable with the 72 hour heat treatments used by Ott and McLaren [30] and the 24 and 96 hour heat treatments utilized by Smart and Glasser.[31]

The addition of P_2O_5 to the 70-30 base glass did not alter the crystalline products of devitrification. X-ray diffraction spectra for the 70-30 glass containing 1.0 mole percent P_2O_5, after extended heat treatment at 400°C and 550°C, are presented in Figure 9. Major peaks can be observed for specimens heat treated for 10 days at 400°C, as shown in curve (a). The positions of these initial peaks agree with the positions of the major peaks of the crystallized 70-30 base glass. The x-ray spectra of the 70-30 base glass and the 70-30-1.0 glass, after devitrification at 550°C, are presented in Figure 10 for comparison. The major peak positions are identical, corresponding to the $3PbO{\cdot}2SiO_2$ polymorph. There are, however, a few differences in the two spectra. The resolution of the three main peaks, with d-spacings of 2.87Å (31.1°), 2.86Å (31.3°), and 2.81Å (31.8°) is not as good in the devitrified 70-30-1.0 composition as it is in the 70-30 composition. Moreover, the peak at 1.81Å (50.5°) and the doublet at 1.87Å (48.7°), observable in the spectra of the 70-30 glass devitrified at 550°C, are missing from the spectra of the 70-30-1.0 composition. These anomalies, however, are also present to some extent in the spectra of the 70-30 composition, since the 1.81Å peak and the 1.87Å doublet became pronounced only in specimens heat treated at 550°C, and are probably due to differences in the extent to which crystallization has progressed. The d-spacings and relative intensities for the major peaks of the 70-30-1.0 composition after devitrification at 550°C are given in Table 1. The results of x-ray diffraction studies of devitrified 70-30-0.5 glass were consistent with those of the devitrified 70-30-1.0 composition.

The x-ray diffraction spectra for the 60-40 base glass are presented in Figure 11. The crystallization process is slower in this glass than in the 70-30 composition, as evidenced by the broad peaks for the 450°C heat treatment, curve (b), compared to the sharp, clearly defined peaks of the 70-30 glass after the same heat treatment, as seen in Figure 8, curve (b). The diffraction spectra of specimens

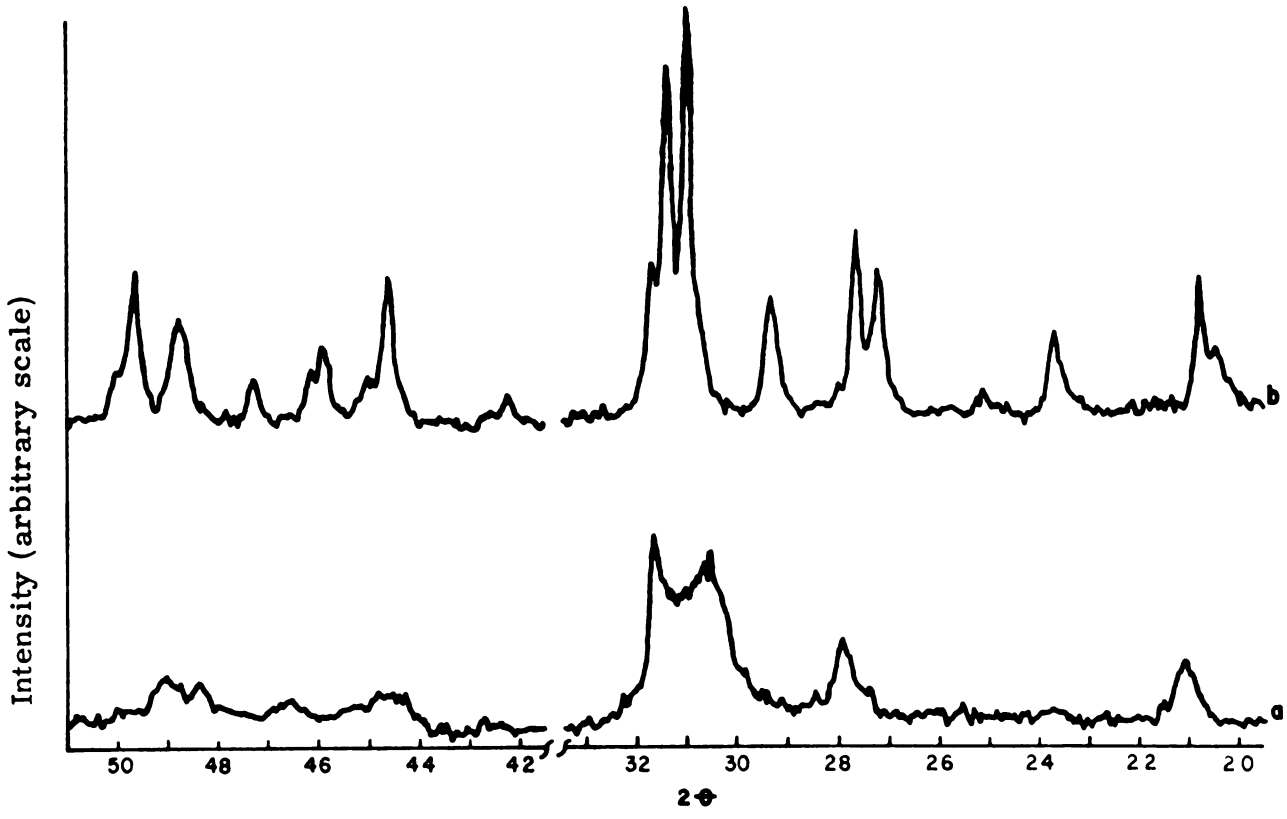

Figure 9. X-ray diffraction spectra of 70-30-1.0 glass devitrified for (a) 10 days at 400°C and (b) 3 days at 550°C.

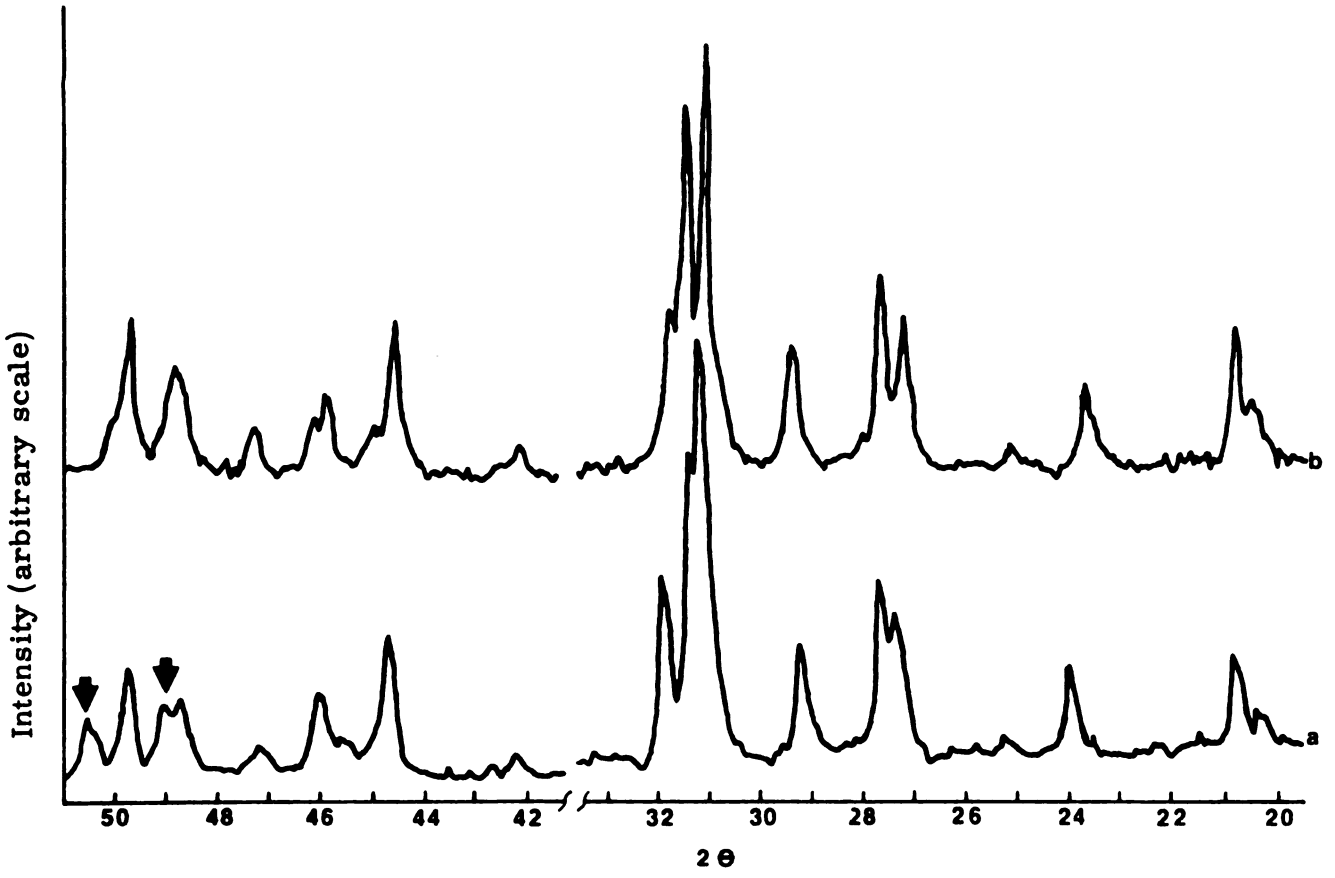

Figure 10. X-ray diffraction spectra of (a) 70-30 glass devitrified for 3 days at 550°C and (b) 70-30-1.0 glass devitrified for 3 days at 550°C. The solid arrows on curve (a) indicate the positions of the additional peaks found in the 70-30 devitrified glass.

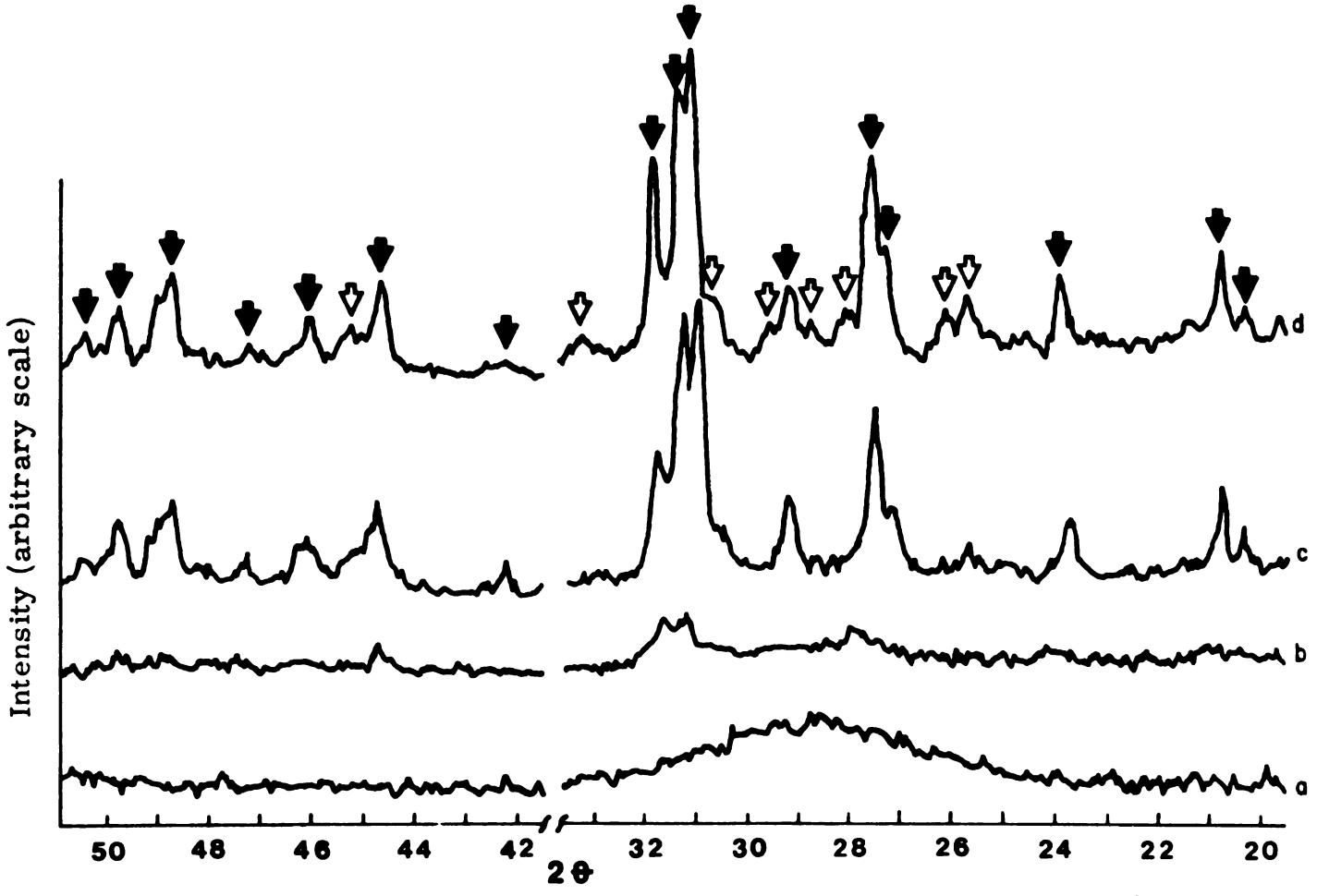

Figure 11. X-ray diffraction spectra of 60-40 glass devitrified for (a) 18 days at 400°C, (b) 6 days at 450°C, (c) 3 days at 500°C, and (d) 3 days at 550°C. The solid arrows along curve (d) indicate the diffraction peaks of the major crystalline phase, and the open arrows indicate the diffraction peaks attributed to the secondary crystalline phase.

crystallized at 550°C show that the major crystalline phase is the same $3PbO{\cdot}2SiO_2$ polymorph that was observed for the 70-30 composition. The peaks attributed to this phase are marked by solid arrows on curve (d), and the d-spacings and relative intensities are given in Table 1. In addition, the devitrified 60-40 glass seems to contain a second crystalline phase, as seen by the additional peaks, marked with open arrows on curve (d). The positions of the peaks suggest that this phase is different from the low-$2PbO{\cdot}SiO_2$ modification found in the devitrified 70-30 glass. Since the 60-40 composition lies to the right of the $3PbO\text{-}2SiO_2$ eutectic on the phase diagrams, it seems reasonable to expect crystallization of a $PbO{\cdot}SiO_2$ compound. Three crystalline forms of composition $PbO{\cdot}SiO_2$ were reported by Smart and Glasser:[31] Alamosite, low-$PbO{\cdot}SiO_2$, and "hexagonal" $PbO{\cdot}SiO_2$. Only Alamosite was considered thermodynamically stable. The x-ray data obtained in this study for the secondary crystalline phase in devitrified 60-40 glass closely resembles that presented by Smart and Glasser[31] for "hexagonal" $PbO{\cdot}SiO_2$. The d-spacings and relative intensities for this phase are listed in Table 3.

The crystallization products of 60-40 glasses were not changed by the presence of P_2O_5. X-ray diffraction spectra for the 60-40-0.5 composition, after heat treatment at 400°C and 550°C are shown in Figure 12, while the corresponding d-spacings and relative intensities are listed in Tables 1 and 3. The major crystalline phase is $3PbO{\cdot}2SiO_2$ (the low temperature modification), while the secondary phase is probably the "hexagonal" $PbO{\cdot}SiO_2$ reported by Smart and Glasser.[31]

5.2 Microstructure of Glasses

Electron microscope examination of the quenched glasses indicated that all glass compositions contained submicroscopic crystals. Representative micrographs taken from replicas of the quenched 70-30 based glasses are shown in Figure 13. Crystals apparently precipitated from the glass during the quenching operation, so that each glass was

Table 3. The d-spacings and relative intensities of the x-ray spectra for the secondary crystalline phase in devitrified 60-40 and 60-40-0.5 glass.

d(Å)	I/I_0	
	60-40(550°C)	60-40-0.5(550°C)
3.46	100	55
3.41	80	45
3.19	90	82
3.10	60	55
3.02	60	36
2.91	100	90
2.69	50	-
2.01	90	100

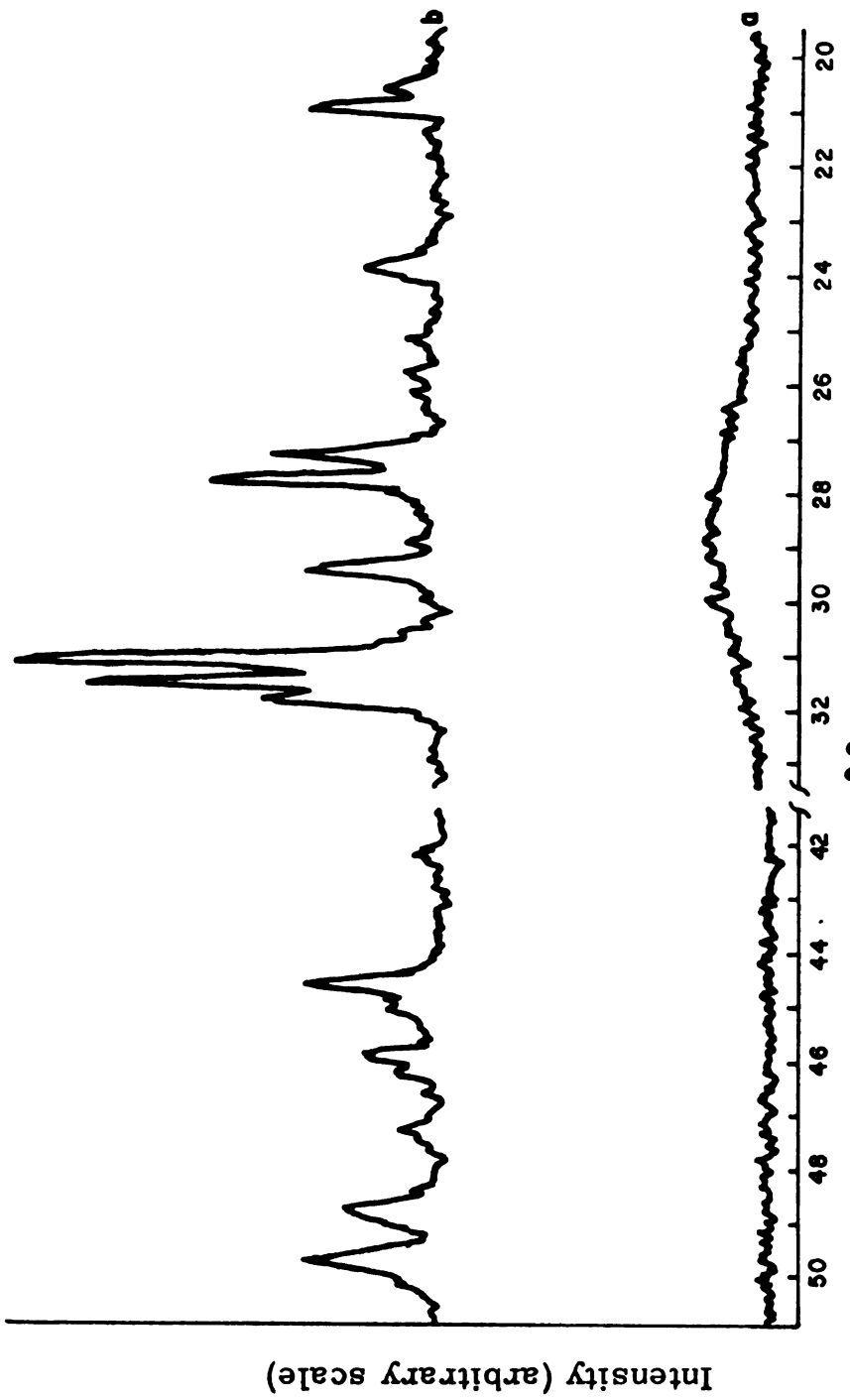

Figure 12. X-ray diffraction spectra of 60-40-0.5 glass devitrified for (a) 18 days at 400°C and (b) 3 days at 550°C.

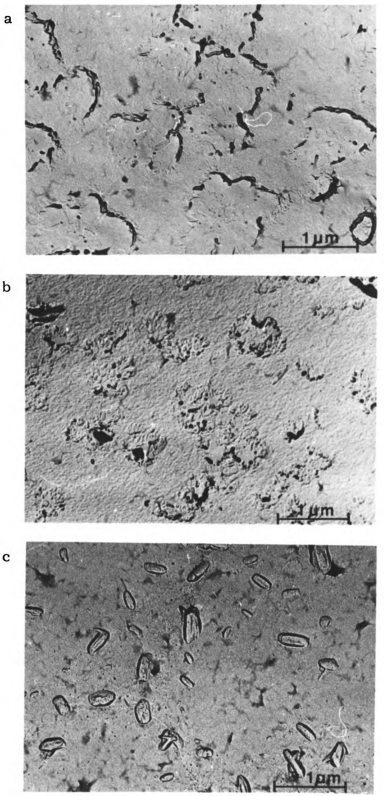

Figure 13. Electron micrographs of replicas of quenched (a) 70-30 glass, (b) 70-30-0.5 glass, and (c) 70-30-1.0 glass.

actually composed of a fine dispersion of crystals amidst a glassy matrix. In the 70-30 and 70-30-0.5 glasses, the crystals occurred in small clusters, whereas in the 70-30-1.0 glass they appeared as lath-like single crystals. In addition to the fine dispersion of crystals, each glass also contained larger regions which were densely crystallized. One such region is shown in Figure 14, for the 70-30-0.5 composition, where a distinct radial growth pattern is evident. Microstructures of the quenched 60-40 based glasses were similar to those of the 70-30 and 70-30-0.5 glasses.

No evidence of widespread phase separation was found for any of the glasses studied. However, some phase separated regions were observed in front of crystalline growth fronts, as seen for example in Figure 15. A narrow phase separated zone separates a heavily crystallized region from the surrounding matrix. Since P_2O_5 is apt to be rejected by growing crystals, the phase separated zone is likely to be of higher P_2O_5 content than the surrounding matrix. If this is the case, then higher concentrations of P_2O_5, e.g. the 2 to 3 mole percent concentrations used by Pavlushkin et al.,[1,2,3] could very well promote phase separation. This would not, however, explain the presence of phase separation in the binary lead silicate glass studied by Vogel.[4] The absence of phase separation noted in this study is in agreement with the expectations reported by Shaw and Uhlmann [5] for lead silicate glasses containing more than 50 mole percent PbO.

Continuation of the crystallization process, through isothermal heat treatment, led to surface crystallization and/or internal crystallization, depending upon the glass composition and the heat treatment temperature. Some degree of surface crystallization was present in all devitrified glasses. Development of the crystalline surface layer was slow at 400°C and began with the formation of discrete crystallites. Micrographs of surface crystals in the 70-30, 70-30-0.5, and 70-30-1.0 glasses after 42 hours of growth at 400°C are presented in Figure 16. As can be seen, the number of crystallites per

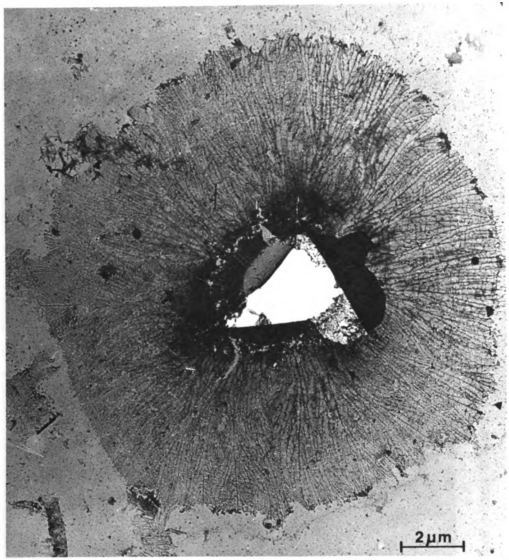

Figure 14. Electron micrograph of radial crystal growth pattern in quenched 70-30-0.5 glass.

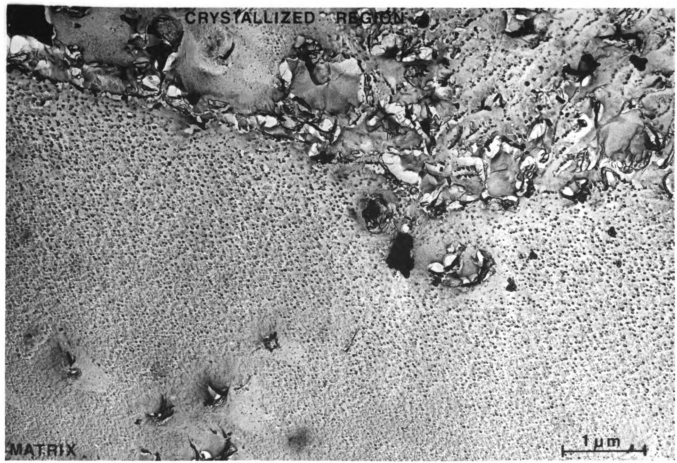

Figure 15. Electron micrograph of phase separated region between crystalline growth front and matrix in quenched 70-30-0.5 glass.

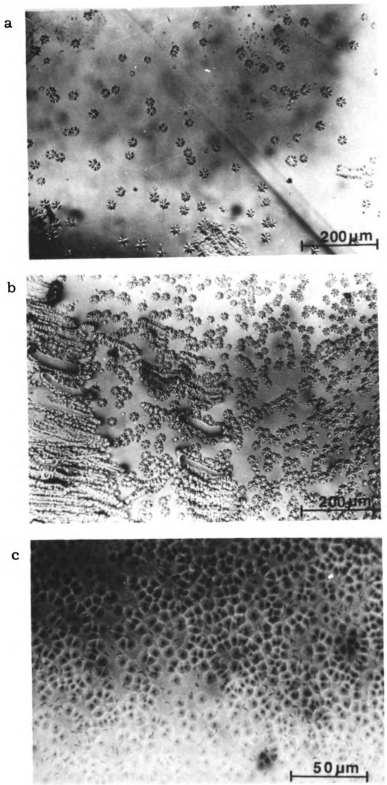

Figure 16. Micrographs of surface crystallites in (a) 70-30 glass, (b) 70-30-0.5 glass, and (c) 70-30-1.0 glass after devitrification at 400°C for 42 hours.

unit area increased significantly with the P_2O_5 content of the glass. Occasionally the crystallites formed in clusters or strung end-to-end as if scratches or other surface irregularities had acted as preferential nucleation sites. In both the 70-30 and 70-30-0.5 glasses, surface crystallites had a distinct radial fiber structure. No such structure was apparent in the surface crystallites of the 70-30-1.0 composition. Possibly the structure is of the same type only on a much finer scale. The 70-30-1.0 composition also contained a number of single crystals, dispersed among the crystallites. These appear as short, dark fibers in Figure 16(c). In all compositions, the surface crystallites grew in both size and number as crystallization continued, and in the 70-30-1.0 composition an increasing number of single crystal fibers appeared. Eventually the glass surface was covered with a crystalline layer. Thereafter, the surface layer grew inward as a unified front. At higher temperatures, the surface crystals grew as lath-like single crystals, as shown in Figure 17. This morphology change was gradual and probably resulted from an aging process. Such a process was reported by Burnett and Douglas [37] for crystallization in the soda-baria-silica system, where a spherulitic structure was observed to disintegrate into detached fibers upon extended heat treatment. Development of the crystalline surface layer in the 60-40 based compositions was similar to that in the 70-30 and 70-30-1.0 glasses.

Although P_2O_5 did not affect the crystallization products of the base glasses, it did have a marked effect on the microstructure of the devitrified glasses. The 70-30 and 60-40 glasses were dominated by surface crystallization at all temperatures studied. These compositions crystallized into fine-grained materials as shown in Figure 18. The faint boundaries commonly seen in these samples, e.g. along AB in Figure 18(a), seemed to result from the intersection of different growth fronts. Occasionally, these compositions contained coarser, more fibrous crystals. At high temperatures, crystallization was

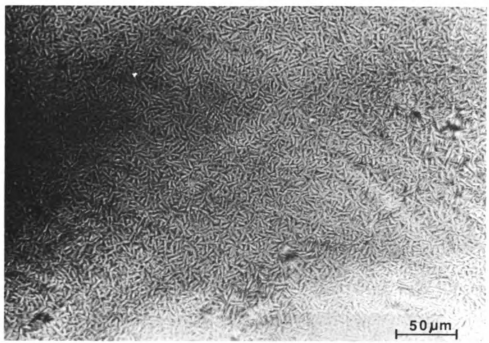

Figure 17. Micrograph of surface crystals in 70-30-0.5 glass after devitrification for 1 hour at 400°C followed by 12 hours at 450°C.

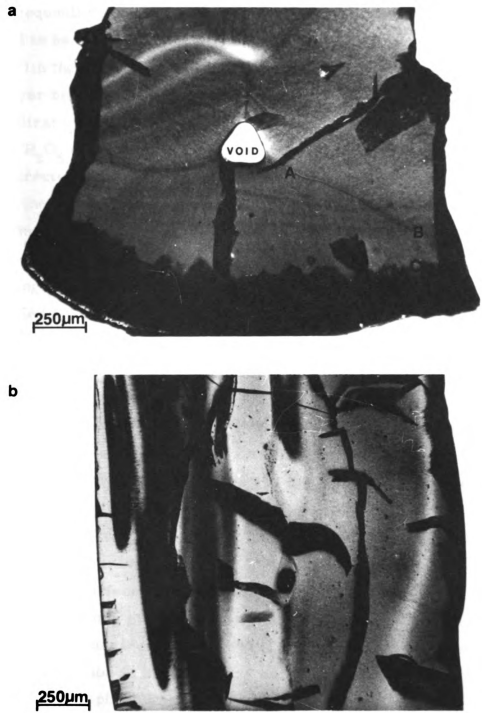

Figure 18. Micrographs of (a) 60-40 glass devitrified at 550°C for 1 hour and (b) 70-30 glass devitrified at 550°C for 72 hours.

rapid and accompanied by extensive deformation and cracking. Voids were frequently observed in these samples, and the devitrified samples seemed to be quite mechanically weak.

With the addition of 0.1 mole percent P_2O_5, the crystalline surface layer became coarser and more fibrous; however, no internal crystallization was observed. The surface layer of all glasses containing P_2O_5 was composed of rather coarse, branched fibers which were directed into the glass interior and which were separated from one another by the same type of finely crystallized material as found in the devitrified base glasses. Figure 19(a), a micrograph of devitrified 60-40-0.1 glass taken with crossed polarizers, shows the branching nature of the fibers, while Figure 19(b), a micrograph of devitrified 60-40-0.5 glass, shows the fine grained material which separated the fibers. The 60-40-0.1 glass was dominated by surface crystallization at all temperatures studied.

In concentrations of 0.5 and 1.0 mole percent, P_2O_5 promoted internal crystallization in the form of spherulites. The number of spherulites nucleated per unit volume was extremely sensitive to both the P_2O_5 concentration of the glass and the crystallization temperature. At 550°C, glasses containing 0.5 mole percent P_2O_5 crystallized completely from the surface, as shown in Figure 20(a) for the devitrified 60-40-0.5 composition. In the 70-30-1.0 composition, however, the advance of the surface layer was limited by the presence of a number of spherulites which grew in the interior of the glass, as shown in Figure 20(b). Heat treatment at 500°C again led predominately to surface crystallization in the 60-40-0.5 and 70-30-0.5 compositions; however, a few spherulites were observed in the interiors of these glasses, as shown in Figure 21 for the 60-40-0.5 composition. In the 70-30-1.0 composition the lowered crystallization temperature resulted in an increased number of spherulites, and hence an even narrower surface layer than was seen for specimens devitrified at 550°C. The number of spherulites per unit volume continued to increase as

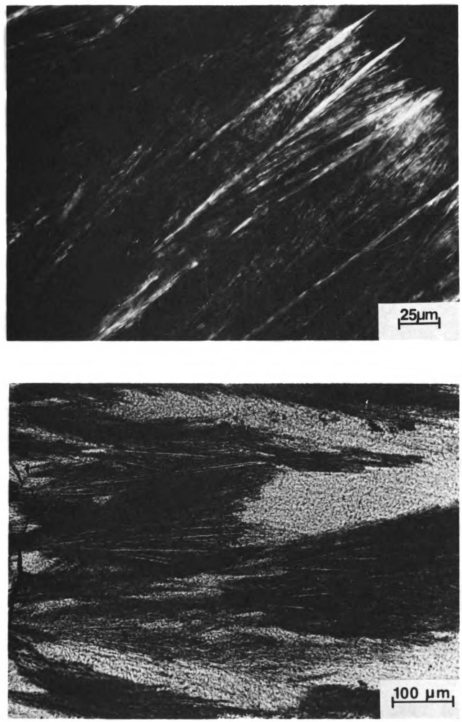

Figure 19. Microstructure of crystalline surface layer in (a) 60-40-0.1 glass devitrified for 1 hour at 550°C and (b) 60-40-0.5 glass devitrified for 72 hours at 550°C.

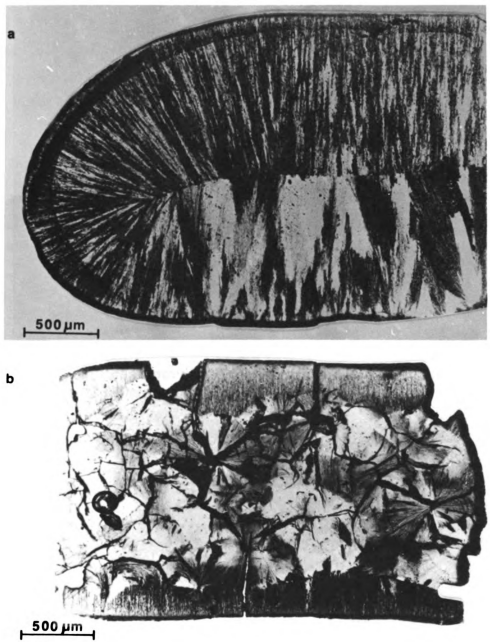

Figure 20. Microstructures after devitrification at 550°C for 72 hours of (a) 60-40-0.5 glass and (b) 70-30-1.0 glass.

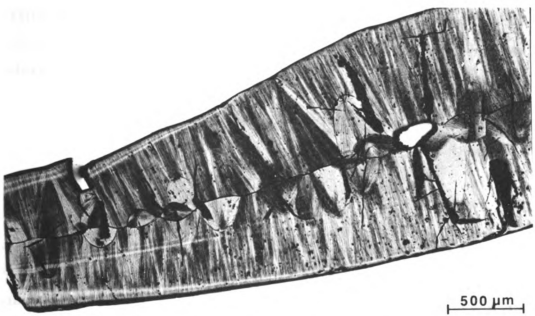

Figure 21. Microstructure of 60-40-0.5 glass after devitrification at 500°C for 72 hours.

the crystallization temperature was lowered, so that at 400°C all of the glasses containing P_2O_5 (except the 60-40-0.1 composition) crystallized with a high concentration of spherulites, as shown in Figure 22. Devitrification at 400°C was significantly more effective at initiating spherulitic growth than devitrification at any of the higher temperatures. The nucleation rates for spherulites at 400°C was determined to be:

Glass Composition	Nucleation Rate(number-cm^{-3}-min^{-1})
70-30-1.0	3.29×10^6
70-30-0.5	2.10×10^4
60-40-0.5	$\sim 3 \times 10^5$

At 450°C, the nucleation rate in the 70-30-1.0 glass dropped to 5.5×10^2 spherulites-cm^{-3}-min^{-1}, while that in the 70-30-0.5 and 60-40-0.5 compositions became too low to measure. Nucleation rates were too low for measurement in all compositions at 500°C and 550°C. Since preliminary investigations indicated that lowering the crystallization temperature to 350°C or 300°C would not further increase the concentration of spherulites, 400°C was taken to be the nucleation temperature for spherulitic growth in the glasses containing P_2O_5.

5.3 Spherulitic Growth Rate

Since the 60-40-0.5 and 70-30-0.5 glasses were dominated by surface crystallization at all temperatures except 400°C, a two-step heat treatment was used for these compositions to study spherulitic growth rates at 450°C, 500°C, and 550°C. In the first step, a heat treatment consisting of 6 hours at 400°C for the 60-40-0.5 composition and 1 hour for the 70-30-0.5 composition was used to induce spherulitic nuclei formation. Then, in the second step, the "nucleated" glasses were heat treated at one of the higher temperatures to produce spherulitic growth. The 70-30-1.0 composition was not given any nucleation treatment, since it displayed some internal

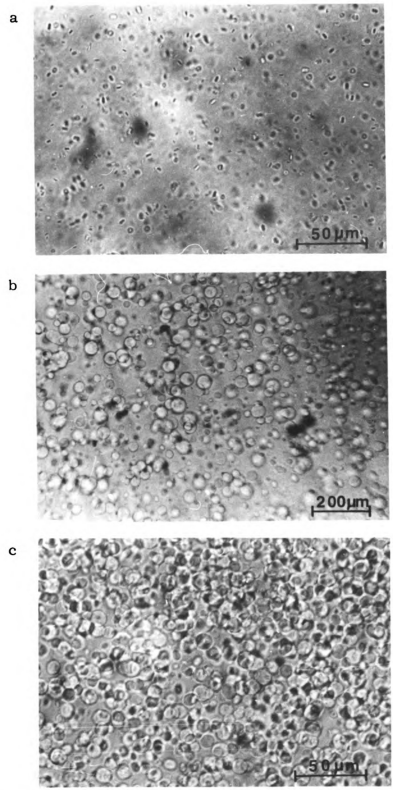

Figure 22. Micrographs of spherulites in (a) 60-40-0.5 glass devitrified for 14 days at 400°C, (b) 70-30-0.5 glass devitrified for 8 days at 400°C, and (c) 70-30-1.0 glass devitrified for 4 days at 400°C.

crystallization at all temperatures; and the 60-40-0.1 composition was not used for spherulitic growth measurements, since even long nucleation treatments at 400°C did not initiate widespread spherulitic growth.

Under isothermal growth conditions, spherulite radii increased linearly with time. Growth curves for crystallization at 400°C, 450°C, 500°C, and 550°C, plotted as the mean spherulite radius versus growth time, are given in Figures 23, 24, and 25 for the 70-30-0.5, 70-30-1.0, and 60-40-0.5 compositions respectively. The nucleation heat treatments given to the 70-30-0.5 and 60-40-0.5 glasses had no significant effect on the determined growth rates, as seen in Figure 25, curve (b), where samples nucleated for 1 hour at 400°C show the same growth rate as those nucleated for 6 hours. Spherulitic growth rates, as determined from the slope of each curve, are given in Table 4. The growth rates were extremely temperature sensitive. Plots of ln(growth rate) versus $(\text{absolute temperature})^{-1}$ are presented in Figure 26, and the activation energy for spherulitic growth, as calculated from the slopes of these plots, is about 80 kcal/mole for all compositions. From viscosity data of Bair,[38] the activation energy for viscous flow in a lead silicate glass containing 60 mole percent PbO can be estimated to be about 84 kcal/mole for temperatures up to and including 400°C. No data was available for the temperature range 400°C to 550°C. Thus, the activation energy for spherulitic growth is close to that required for viscous flow in binary lead silicate glass.

Among the glasses containing P_2O_5, growth was much more rapid in the 70-30 based glasses than it was in the 60-40 based glasses. P_2O_5, itself, markedly effected the spherulitic growth rate. Increased concentrations of P_2O_5 slowed spherulite growth substantially, as seen by comparing the growth rates for the 70-30-0.5 and 70-30-1.0 compositions. Although no quantitative data was obtained for the base compositions, observations of surface layer growth, indicated that

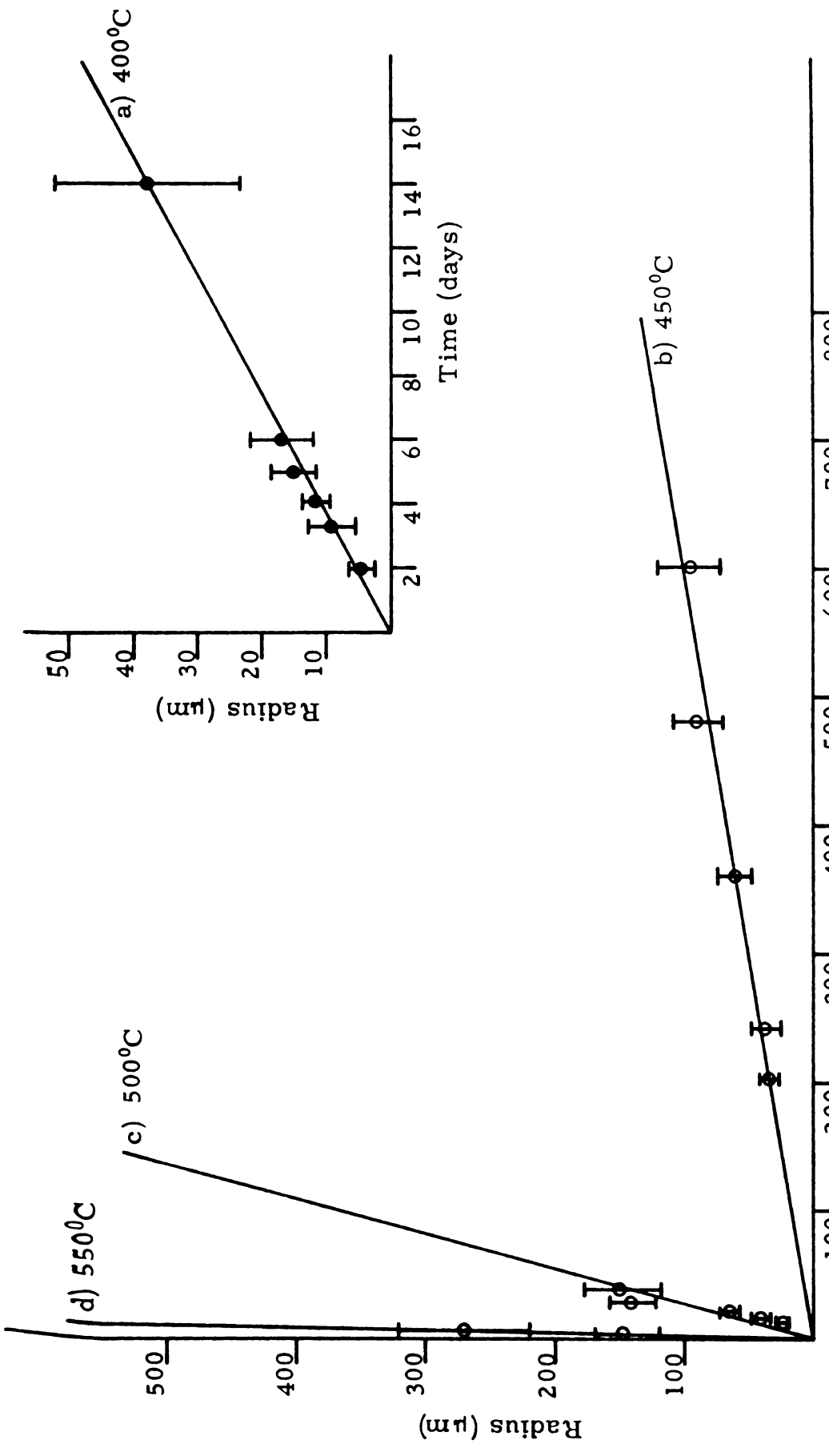

Figure 23. Growth curves for spherulites in 70-30-0.5 glass at (a) 400°C, (b) 450°C, (c) 500°C, and (d) 550°C. (o -- samples nucleated for 1 hour at 400°C; ● -- samples given no nucleation)

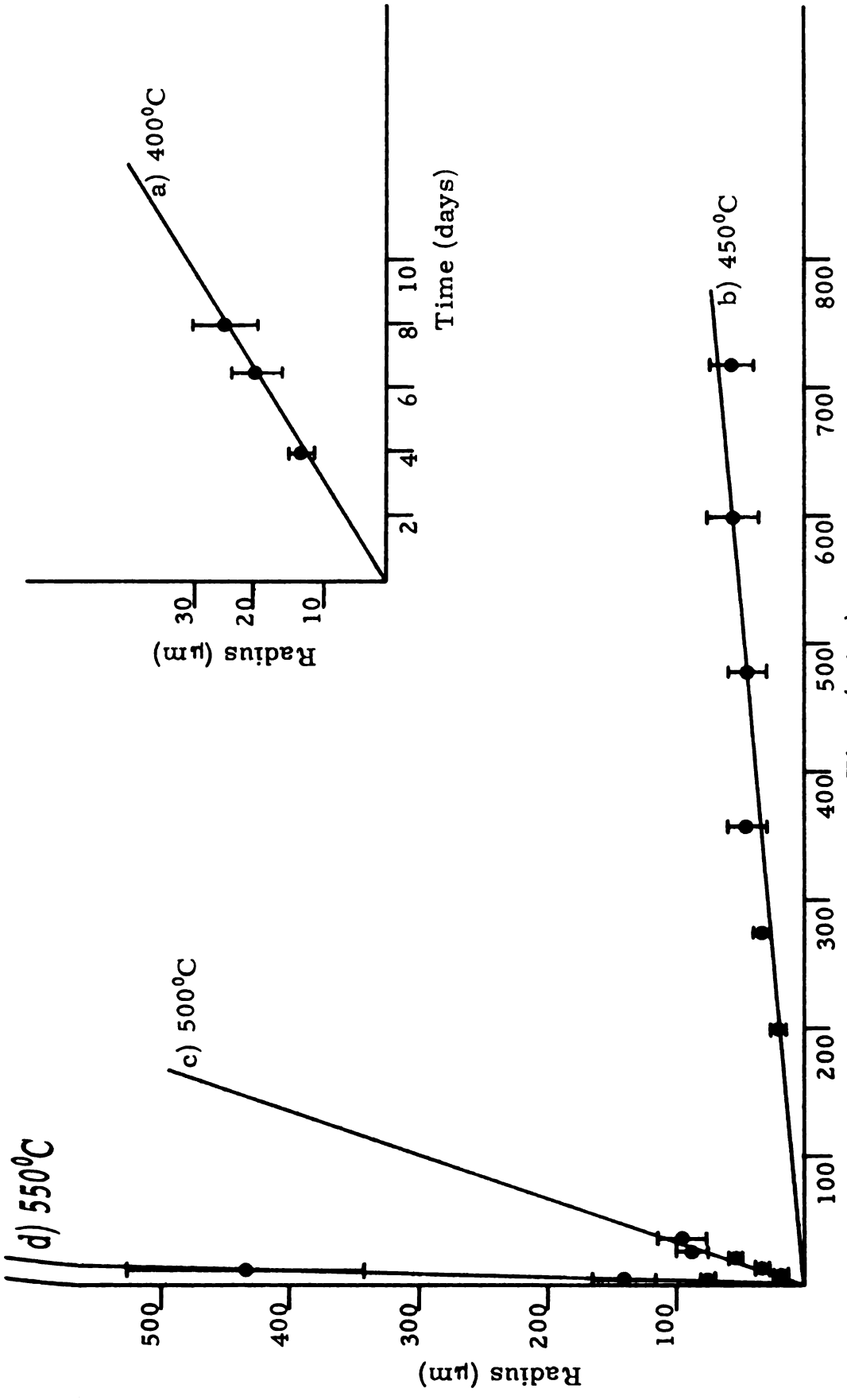

Figure 24. Growth curves for spherulites in 70-30-1.0 glass at (a) 400°C, (b) 450°C, (c) 500°C, and (d) 550°C.

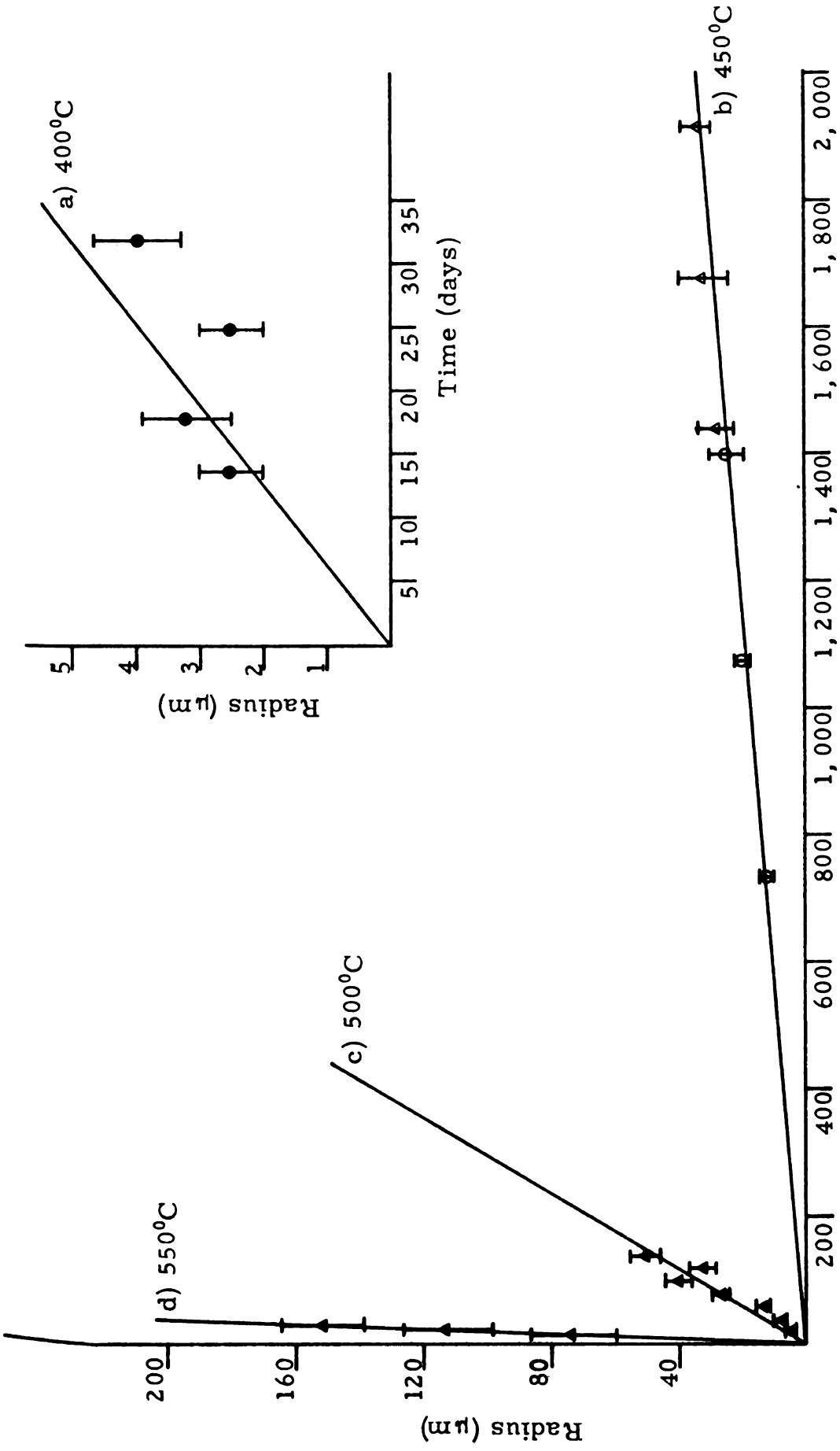

Figure 25. Growth curves for spherulites in 60-40-0.5 glass at (a) 400°C, (b) 450°C, (c) 500°C, and (d) 550°C. (▲ -- samples nucleated for 6 hours at 400°C; o -- samples nucleated for 1 hour at 400°C; and ● -- samples given no nucleation)

Table 4. Crystal growth rate* as a function of temperature and glass composition.

TEMPERATURE	COMPOSITION		
	70-30-0.5	70-30-1.0	60-40-0.5
400°C	0.0017	0.0009	0.0001
450°C	0.16	0.10	0.021
500°C	5.12	2.97	0.40
550°C	60.2	52.4	5.26

* growth rates are presented in units of $\mu m\text{-}min^{-1}$

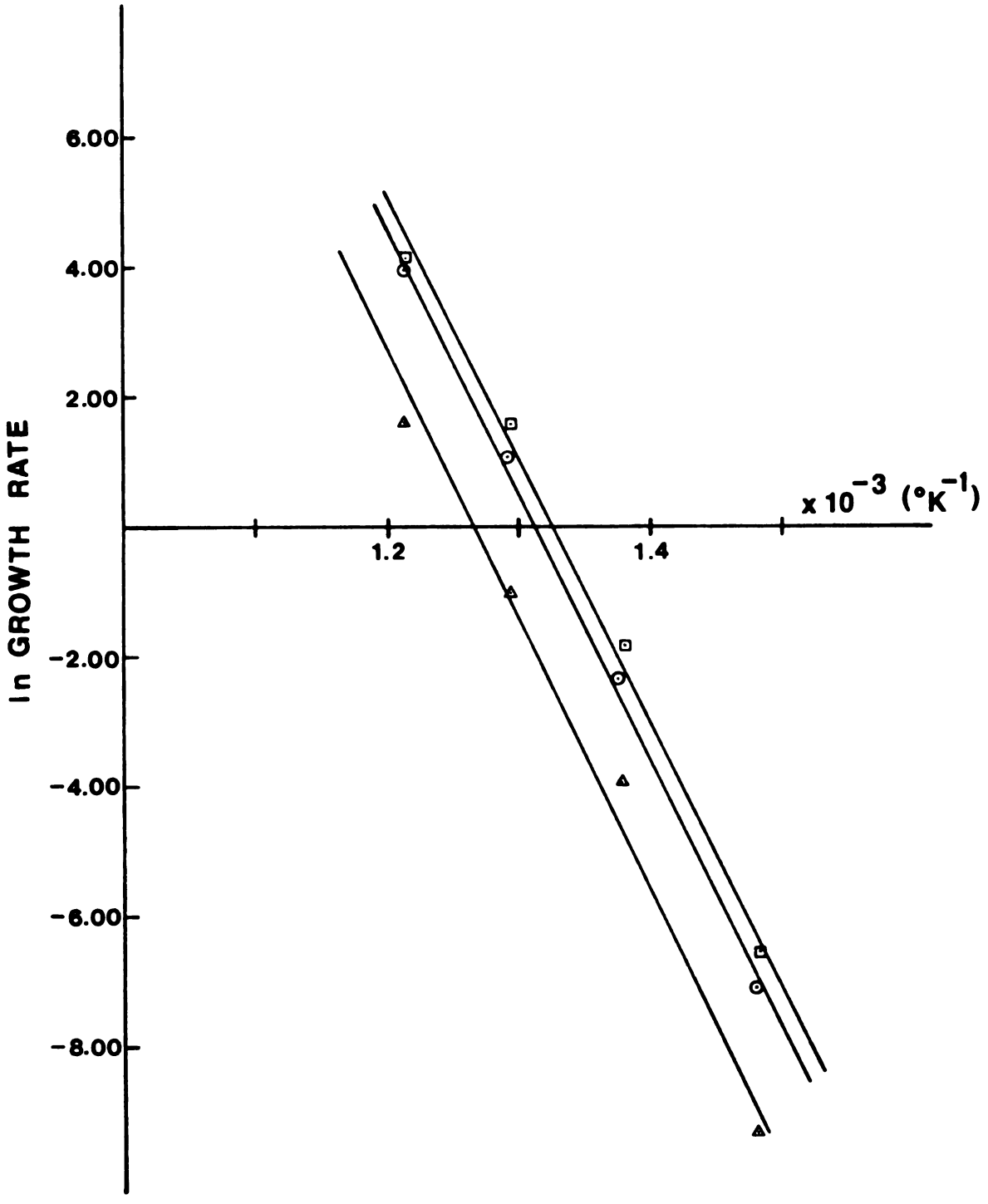

Figure 26. Graph of ln(crystal growth rate) versus the reciprocal of the absolute temperature. (Data points for the 70-30-0.5, 70-30-1.0, and 60-40-0.5 compositions are plotted as squares, circles, and triangles, respectively)

crystal growth was even faster in the base glasses than in the P_2O_5 glasses.

Histograms, showing the size distribution of spherulite populations after isothermal crystallization, are presented in Appendix A. Comparison of these histograms shows that for each composition:

(1) the upper boundary (the largest size) of the spherulite population increased with isothermal growth time, while

(2) the lower boundary (the smallest size) remained approximately constant with time for growth at 400°C and began to increase more and more with time as the growth temperature was raised. The inability of each composition to keep the lower size intervals filled at higher temperatures as crystallization progresses substantiates earlier observations that the nucleation process for spherulitic growth is inhibited at temperatures above 400°C.

5.4 Spherulitic Morphology

Spherulites observed in this study were composed of arrays of crystalline fibers, arranged radially outward from a common center. Growth occurred through a lengthening of the fibers and was accompanied by fiber branching, which tended to "fill-in" the interior of the spherulite and trap matrix material between the fibers. The width of the fibers and the degree to which they branched varied with the growth temperature.

At 550°C, spherulites grew with coarse, open textures. Three basic morphologies could be distinguished, as shown in the micrographs presented in Figure 27. The spherulite in Figure 27(a) is characterized by an elongated major axis from which fibers fan out on either side, creating a sheaf-like appearance. In Figure 27(b), the spherulite is seen as a bundle of more-or-less parallel fibers, while in Figure 27(c), it takes on a distinctly hexagonal shape. These different morphologies were found to arise not from three different growth patterns, but rather from three different views of the same

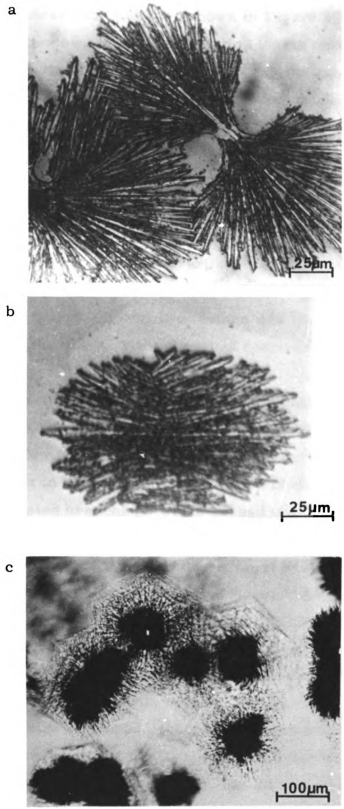

Figure 27. Spherulites grown at 550°C showing typical (a) sheaf, (b) bundle, and (c) hexagonal morphologies.

growth pattern, so that when a spherulite is oriented as shown in Figure 28, the three morphologies shown in Figure 27(a), (b), and (c) correspond to views along the x, y, and z axis respectively.

As the growth temperature was lowered, the spherulites became more spherical in shape, and the fibers became much finer. Figure 29 is a micrograph of spherulites in the 70-30-0.5 composition after growth at 450°C. The distinct sheaf-like shape observed in spherulites grown at 550°C is not seen in spherulites grown at 450°C; however, a slight sheaf-like arrangement of fibers can still be detected. In spherulites grown at 400°C, the fiber structure was no longer resolvable with light microscopy. However, an electron micrograph showing the fibrous growth morphology of spherulites grown at 400°C is presented in Figure 30. Spherulite texture was also effected by the P_2O_5 content of the glass, with increased concentrations of P_2O_5 producing finer spherulitic textures.

Several growth stages were observed in spherulites crystallized at 550°C or 500°C. In the earliest stages of growth, spherulites consisted of just a few fibers, or platelets, which spread out slightly from center, as shown in Figure 31. Development of these spherulites continued with repeated branching, which caused the fibers to fan out more from center, forming fuller sheaves. Figure 32, an electron micrograph of the outer tips of a spherulite grown at 550°C in 60-40-0.5 glass, shows the branching nature of the fibers. As growth continued, branching fibers gradually encircled regions on either side of center, forming eye-like regions made up of trapped matrix, as shown in Figure 33. At lower temperatures, spherulite morphology did not change significantly with growth, as even the smallest spherulites observed had a fully developed, spherically symmetric appearance, indicating that the development stage was completed while the spherulites were still of submicroscopic size. At all temperatures, a spherulite's radial growth continued until halted by its impingement with neighboring spherulites. In this way a polyhedral network of

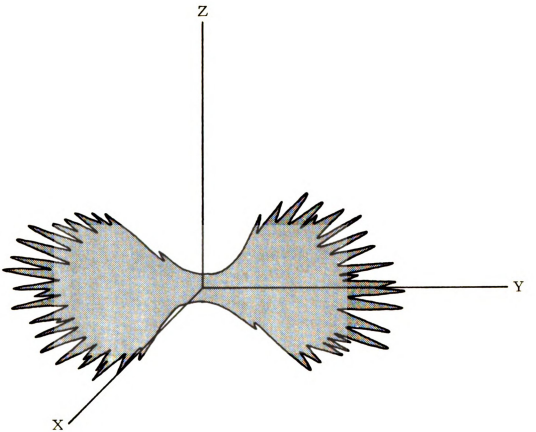

Figure 28. Diagram of spherulite orientation.

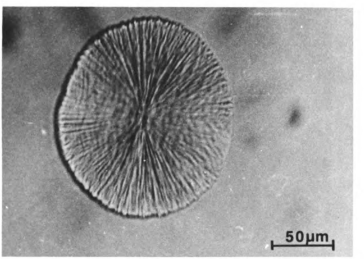

Figure 29. Micrograph of a spherulite in 70-30-0.5 glass after growth at 450°C.

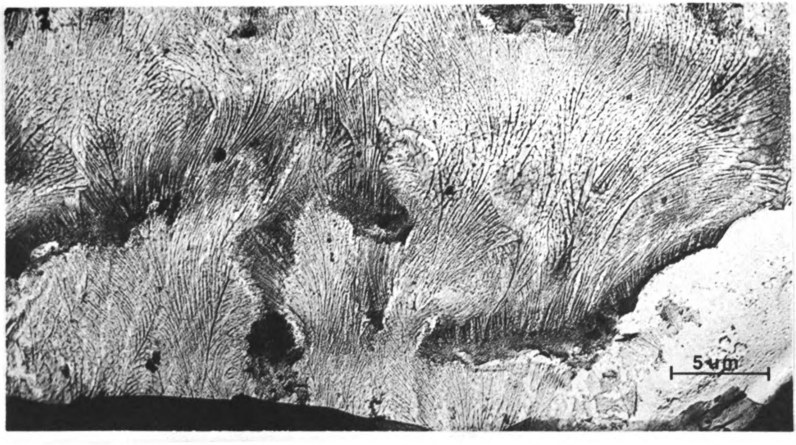

Figure 30. Electron micrograph of fibrous growth morphology in spherulites grown at 400°C in 70-30-0.5 glass.

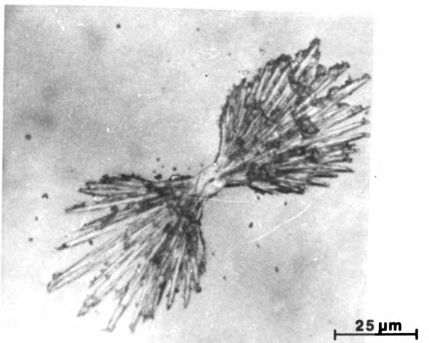

Figure 31. Micrograph of an early growth stage in a spherulite grown at 550°C.

Figure 32. Electron micrograph of branching fibers in a spherulite grown at 550°C.

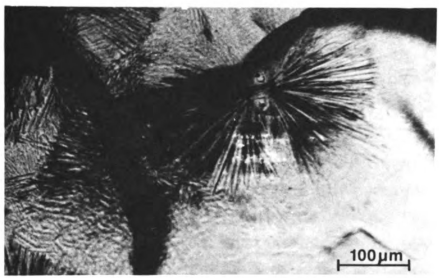

Figure 33. Micrograph of a mature spherulite grown at 550°C.

inter-spherulitic boundaries was formed in highly crystallized samples, as shown in Figure 34 for the 70-30-0.5 composition. Matrix trapped inside the spherulite gradually crystallized, producing the fine-grained texture.

5.5 Role of P_2O_5

Our investigations show that, as reported by Pavlushkin et al.,[1,2,3] P_2O_5 is effective in promoting bulk crystallization in lead silicate glasses containing between 50 and 60 mole percent PbO. The presence of P_2O_5 in sufficiently high concentrations (0.5 mole percent for the two glass compositions studied) leads to the creation of internal nucleation sites from which spherulitic growth occurs. The exact role played by P_2O_5 in promoting spherulitic growth is, however, unclear. Since the addition of 0.1 mole percent P_2O_5 led to a more fibrous growth morphology, but not to spherulitic nucleation, the role of P_2O_5 may be two-fold, namely (1) to nucleate internal crystals of the major crystalline phase, $3PbO{\cdot}2SiO_2$ and (2) to promote a fibrous growth morphology. Pavlushkin et al.[3] proposed that the presence of P_2O_5 led to phase separation followed by the formation of crystalline nuclei. Since no evidence of widespread phase separation was found in this study, it seems unlikely that phase separation (even though it may occur with higher P_2O_5 concentrations) is a pre-requisite for internal nucleation in these glasses. Furthermore, the matrix crystals, present in the quenched glasses, do not seem to promote internal crystallization of the major crystalline phase. The fact that no phosphorus compounds were observed during devitrification, coupled with the observation the P_2O_5 led to greatly reduced spherulitic growth rates, suggests that P_2O_5 may be acting solely as an impurity in these glasses, promoting internal nucleation by reducing the interfacial energy between the glass and the crystal. Such a role was suggested by James and Keown [39] to explain the increased nucleation rate of

Figure 34. Network of inter-spherulitic boundaries in a completely devitrified 70-30-0.5 glass. The arrows indicate the boundary network.

spherulites in lithium silicate glasses containing 1 mole percent P_2O_5.

Recently, crystal growth morphologies have been examined in relation to the entropy of fusion, and the importance of this parameter in predicting crystal-liquid interface structure and crystal morphology has been demonstrated.[40, 41, 42, 43] Jackson [40, 41, 42] calculated the free-energy change associated with the addition of atoms to available sites on growth interfaces of crystals. According to his model, the surface free-energy change can be expressed in terms of a parameter α, which can be written as

$$\alpha = \frac{\Delta S_{fm}}{R} \zeta \quad ,$$

where ΔS_{fm} is the entropy of fusion, R is the universal gas constant, and ζ is the fraction of total bonding energy contributed by the addition of atoms at adjacent sites on the surface. ζ, always less than unity, depends upon the structure of the crystal growth face, being largest for the most closely-packed planes. The surface free energy was found to vary with α as shown in Figure 35. The position of the minima depends upon the value of α. For $\alpha < 2.0$, the minimum free-energy change occurs for half of the available surface sites being filled, which is representative of a growth surface which is rough on an atomic scale. For $\alpha > 2.0$, however, minima in the surface free-energy change occur for surfaces in which there are either a very small or very large fraction of filled sites, which corresponds to a growth plane which is smooth on an atomic scale. Since,

$$\alpha = \frac{\Delta S_{fm}}{R} \zeta \quad ,$$

the $\alpha < 2$ situation occurs for

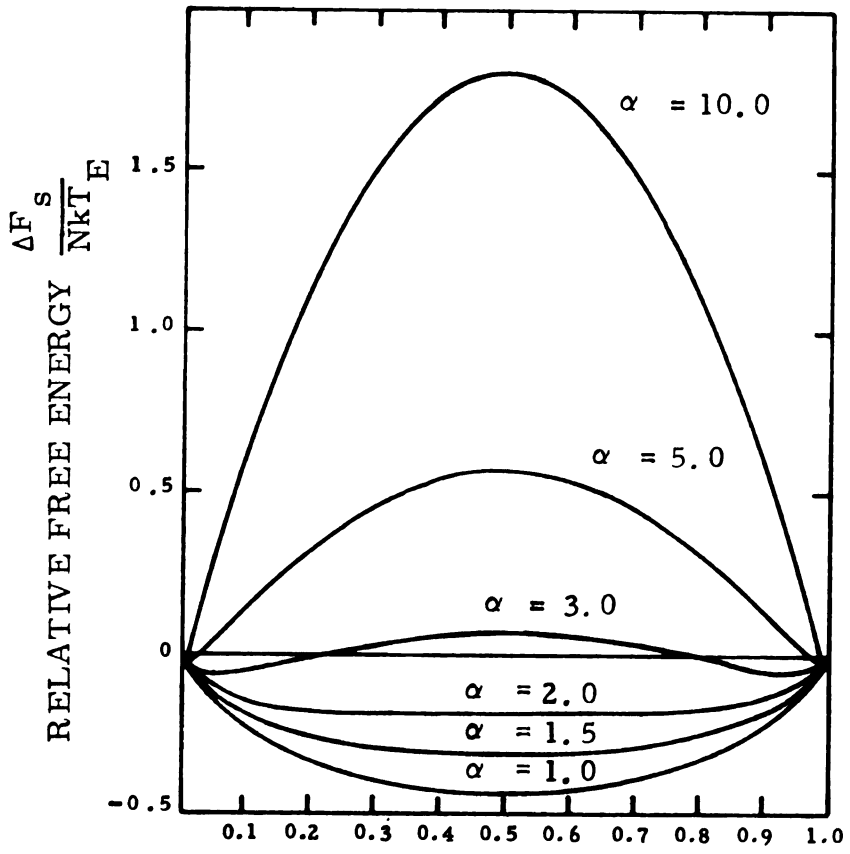

Figure 35. Free energy of an interface versus occupied fraction of surface sites.[42]

$$\frac{\Delta S_{fm}}{R}\zeta < 2 \quad ,$$

or,

$$\Delta S_{fm} < \frac{2R}{\zeta} \quad .$$

Since $\zeta < 1$, materials with $\Delta S_{fm} < 2R$ fall into the $\alpha < 2$ category, and are expected to crystallize with "atomically" rough surfaces and exhibit low growth rate anisotropy and non-faceted morphologies. The $\alpha > 2$ situation occurs for

$$\Delta S_{fm} > \frac{2R}{\zeta} \quad .$$

Since ζ is ≥ 0.5 for close-packed planes, materials having $\Delta S_{fm} > 4R$ are expected to crystallize with "atomically" smooth surfaces for close-packed planes (which corresponds to the $\alpha > 2$ situation) and rougher surfaces along less closely packed planes (where α falls below 2 due to the decreasing ζ). For these materials, a high growth-rate anisotropy and a faceted morphology along close-packed planes is also expected.

Materials with high entropies of fusion may also, according to Uhlmann,[43] be expected to have growth rates not well described by the standard models for crystal growth. These materials often show a tendency towards spherulitic growth at large undercoolings, which become even more pronounced in the presence of impurities. The growth morphologies observed in this study closely match those predicted by Jackson and Uhlmann for materials with high entropies of fusion. Based on Shartsis and Newman's [44] study of energy relations in the $PbO\text{-}SiO_2$ system, the entropy of fusion for $3PbO \cdot 2SiO_2$ can be estimated to be approximately 4.3R. In the base glasses and the

60-40-0.1 composition, where spherulitic growth was not observed, a faceted growth morphology was apparent, as seen in Figure 36. As the P_2O_5 concentration was increased, the tendency towards spherulitic growth became more pronounced, finally becoming the preferred mode of crystallization with the addition of 1.0 mole percent P_2O_5.

Certain morphological features and growth patterns have been found to be characteristic of spherulitic crystallization, irrespective of the system in which crystallization occurs. Typically, spherulites are composed of fibers which radiate outward from a common center. The fibers are of approximately constant thickness and have a preferred crystal axis along the radial direction. Fiber thickness increases with increased growth temperature and decreases with increased impurity content. The fibers are separated from one another by uncrystallized melt. Spherulitic development proceeds from bundles of parallel fibers which fan out to form intermediate structures called sheaves. As growth continues a spherical shape gradually develops. Spherulitic growth rates, characteristically, are constant with time under isothermal conditions.

A theory to account for spherulitic crystallization has been presented by Keith and Padden.[45] Two properties, high viscosity and the presence of impurities, are seen as fundamental to spherulite formation. The presence of impurities in melts with high viscosities, and low growth rates, leads to the build-up of a narrow impurity rich layer ahead of the growing crystal, which causes the interface to become unstable with respect to pertubations. Fibrous growth results, with the fiber thickness determined by δ, the thickness of the interface. δ is approximated as D/G, where D is the diffusion coefficient for the impurity in the melt and G is the growth rate. The variation in fiber thickness with growth temperature, characteristic of spherulites, is explained in terms of the change of δ with temperature. At large undercoolings, δ is small, leading to relatively narrow fibers. As the

Figure 36. Electron micrograph of faceted crystal growth in a 60-40-0.1 glass after devitrification at 450°C for 1 hour.

crystallization temperature is raised δ increases, and the fiber width broadens. Once fibrous growth is established the spherulite morphology can result, through the sheaf-to-spherulite development sequence, provided that a source of branching is present. Branching is seen as resulting from the encounter of a growing fiber with any singularity or region of disorder whose size is comparable with δ. As δ decreases, the frequency of branching is assumed to increase due to the greater probability of encounters with singularities large enough to cause branching. Thus, the size at which the sheaf-to-spherulite transformation occurs is expected to decrease as the spherulite's texture becomes finer, with the more frequent branching, expected for narrower fibers, leading to a more rapid spherulite development.

The spherulite morphologies and growth patterns observed in this study were consistent with those characteristic of spherulites in general. The theory of spherulitic growth proposed by Keith and Padden [45] can account reasonably well for the spherulitic growth observed in this study, and the implication is again that P_2O_5 functions as an impurity in these glasses. Therefore, it seems likely that the crystallization behavior observed in the glasses containing P_2O_5 results from its role as an impurity -- increasing the internal nucleation rate by reducing the interfacial energy between the glass and the crystal and promoting a spherulitic morphology by enhancing fibrous growth.

CHAPTER VI

SUMMARY

1. Concentrations as low as 0.5 mole percent P_2O_5 promoted internal crystallization in the lead silicate glasses studied. Internal crystallization initiated from discrete centers within the glass and exhibited a spherulitic morphology.
2. No evidence of widespread phase separation was found in any of the glasses. This was unexpected on the basis of the work of Pavlushkin et al.[3] and Vogel.[4] All quenched glasses were, however, partially crystallized, containing dispersions of submicroscopic size crystals.
3. In the low concentrations studied, P_2O_5 had no detectable effect on the phases which occurred as crystallization products. The major crystalline phase in all devitrified glasses was a low temperature polymorph of $3PbO \cdot 2SiO_2$. Secondary products of crystallization were tenatively identified as low-$2PbO \cdot SiO_2$ in the 70-30 based glasses and "hexagonal" $PbO \cdot SiO_2$ (a polymorph of $PbO \cdot SiO_2$ reported by Smart and Glasser[31]) in the 60-40 based glasses.
4. 400°C was found to be the most effective temperature for nucleating spherulitic growth. Devitrification at this temperature led to high concentrations of spherulites in all glasses containing at least 0.5 mole percent P_2O_5. Concentrations of 1.0 mole percent P_2O_5 were needed to produce detectable levels of spherulitic nucleation at temperatures above 400°C.
5. Spherulitic radii increased linearly with time under isothermal conditions. Spherulitic growth rates increased with increased crystallization temperature, showing an experimental activation

energy of about 84 kcal/mole. Increased concentrations of P_2O_5 led to decreased spherulitic growth rates.

6. Spherulites observed in this study exhibited morphological features and growth patterns characteristic of spherulites found in polymers and other materials. Spherulite morphology developed through the sheaf-to-spherulite sequence, and spherulite texture coarsened and became more open as the growth temperature was increased. The observed features were consistent with Keith and Padden's[45] theory of spherulitic growth.
7. The entropy of fusion of base glasses studied was estimated to be about 4.3R, where R is the universal gas constant. The spherulitic growth habit was in accord with the prediction of Jackson[42] and Uhlmann[43] for materials with entropies of fusion greater than 2R.
8. The crystallization behavior observed in this study can be explained on the basis of P_2O_5 acting as an impurity since it increased the internal nucleation rate and promoted spherulitic crystal growth.

APPENDIX

APPENDIX A

HISTOGRAMS OF SPHERULITE POPULATIONS IN DEVITRIFIED GLASSES

The sizes of spherulites in devitrified glass samples were studied by light microscopy. The diameters of spherulites in each sample were measured from micrographs taken at random intervals over the sample. This data was used to construct histograms showing the total number of spherulites observed in each size in the devitrified sample. Since most of the data was obtained from photographs taken at a magnification of 75X, the size intervals on the histograms are presented as 75X the actual spherulite diameter. Histograms of spherulite populations occurring in 70-30-0.5, 70-30-1.0, and 60-40-0.5 glasses after extended heat treatments at 400°C are presented in Figures A.1, A.2, and A.3 respectively. As the heat treatment time was extended at 400°C, the spherulites in each glass grew in size, occupying higher size intervals. However, the lower size intervals also remained filled. Histograms of spherulite populations in 70-30-0.5, 70-30-1.0, and 60-40-0.5 glasses after growth at 450°C are presented in Figures A.4, A.5, and A.6 respectively. Those of spherulite populations in 70-30-0.5, 70-30-1.0, and 60-40-0.5 glasses after growth at 500°C are given in Figures A.7, A.8, and A.9 respectively; while those of spherulite populations in 70-30-0.5, 70-30-1.0, and 60-40-0.5 glasses after growth at 550°C are presented in Figures A.10, A.11, and A.12. As the growth temperature was increased from 400°C, there was a tendency for the lower size intervals to empty, as the higher intervals filled. It is clear from the histograms of spherulite populations in these glasses at 450°C, 500°C, and 550°C (Figures A.4 through A.12) that no significant amount of spherulite

nucleation occurred during growth at these temperatures.

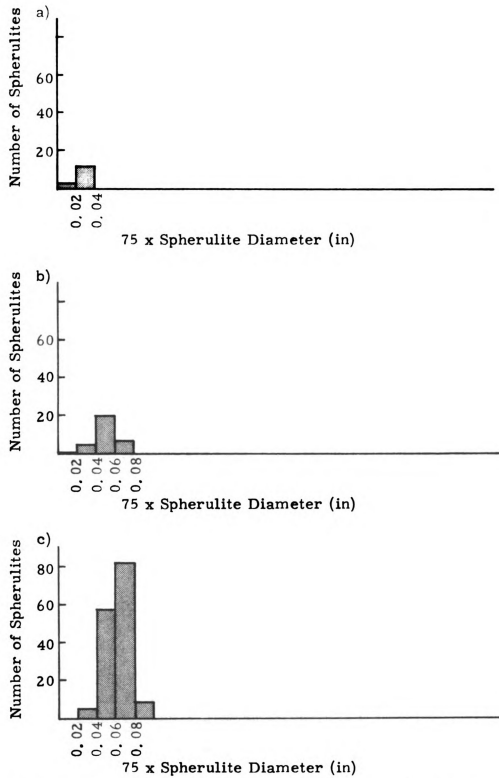

Figure A. 1. Histograms of spherulites grown in 70-30-0. 5 glass at 400°C for (a) 2 days, (b) 3¼ days, (c) 4 days, (d) 5 days, (e) 6 days, and (f) 14 days.

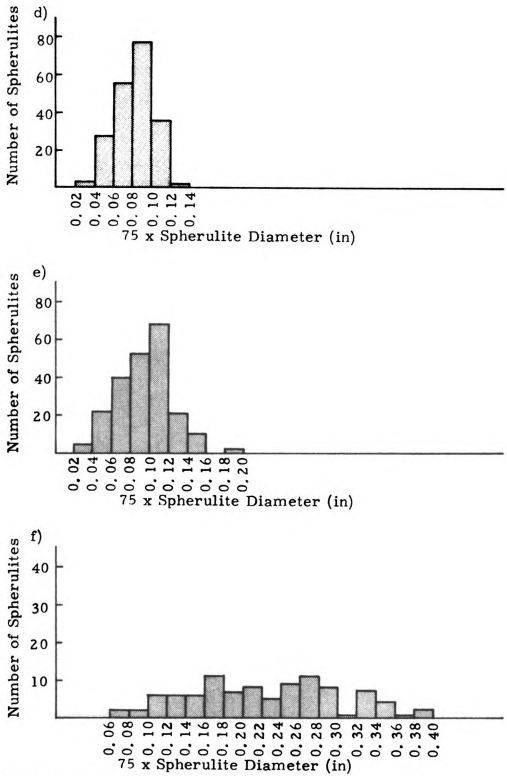

Figure A. 1. cont.

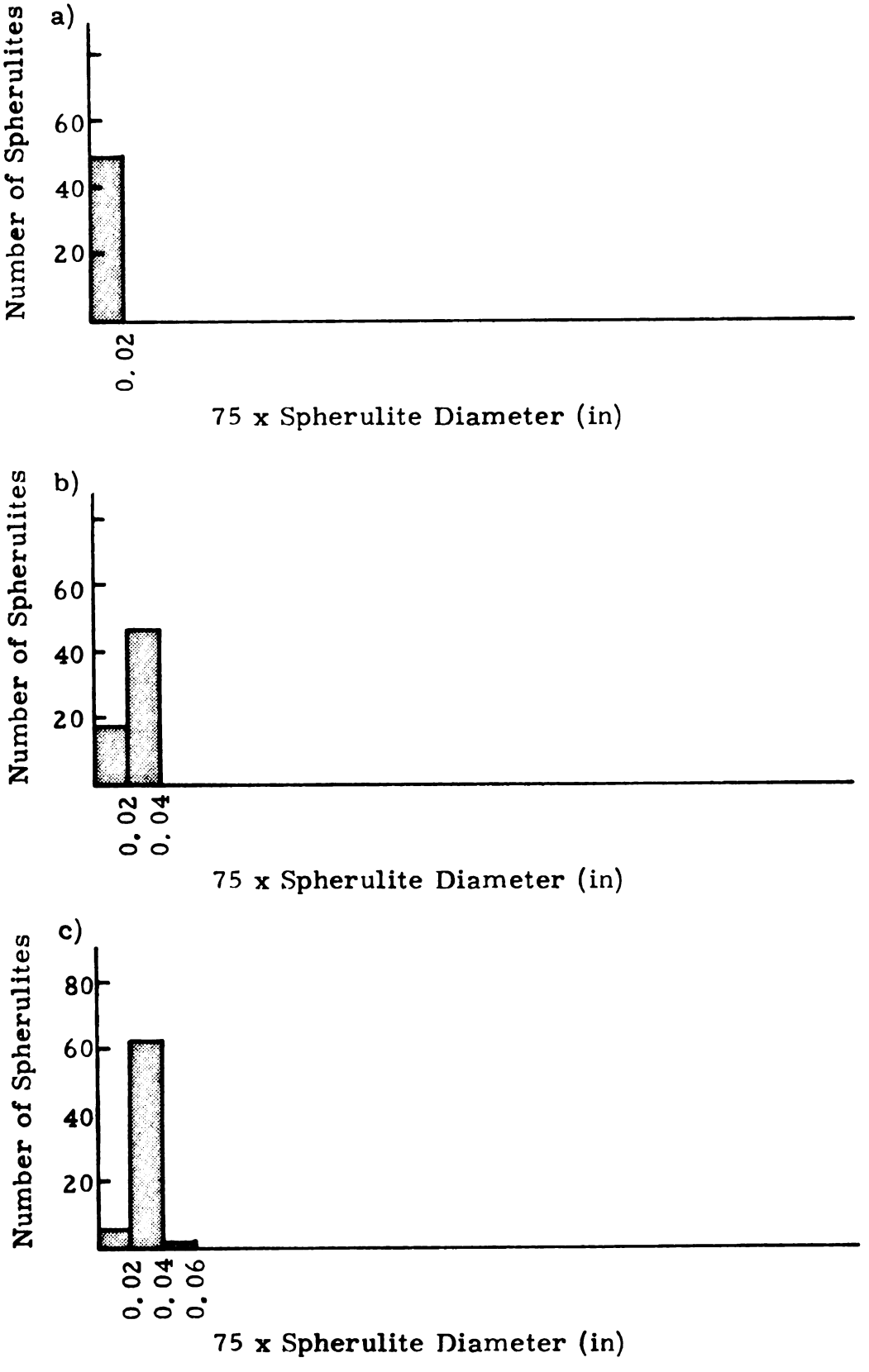

Figure A. 2. Histograms of spherulites grown in 70-30-1.0 glass at 400°C for (a) 2 days, (b) $3\frac{1}{4}$ days, and (c) 4 days.

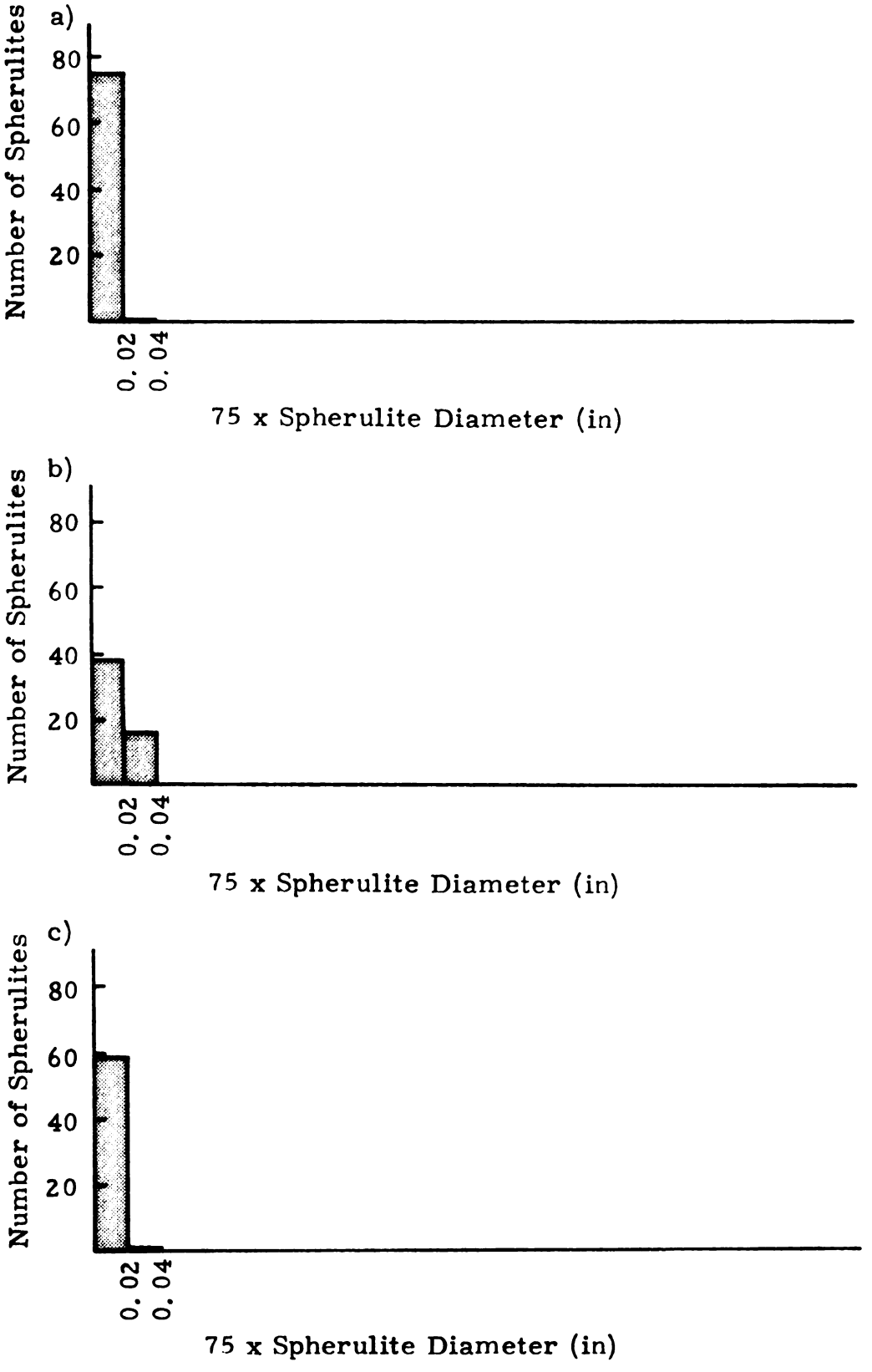

Figure A. 3. Histograms of spherulites grown in 60-40-0.5 glass at 400°C for (a) 14 days, (b) 18 days, (c) 25 days, and (d) 32 days.

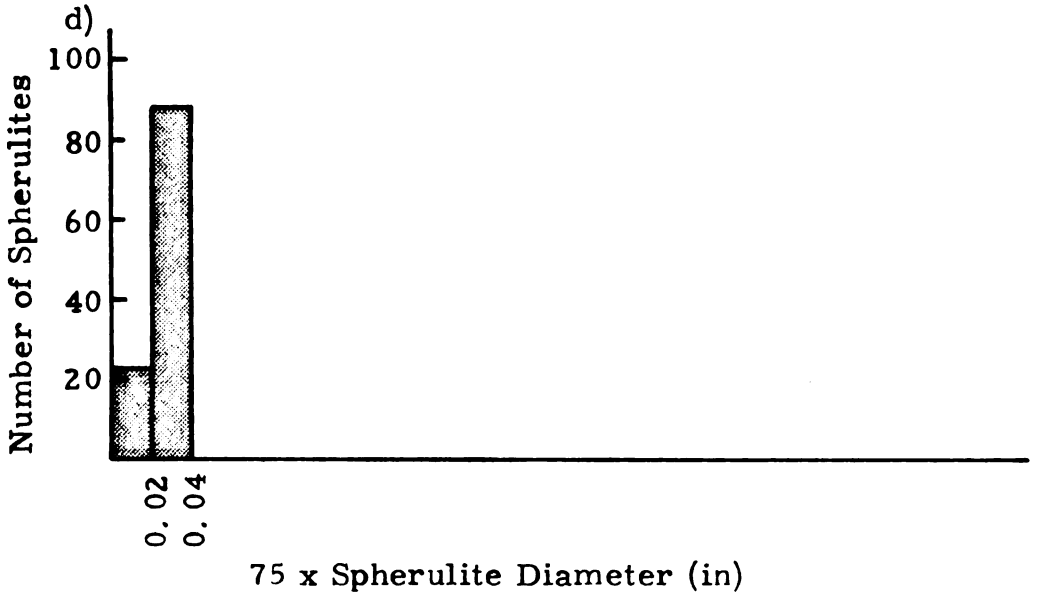

Figure A.3. cont.

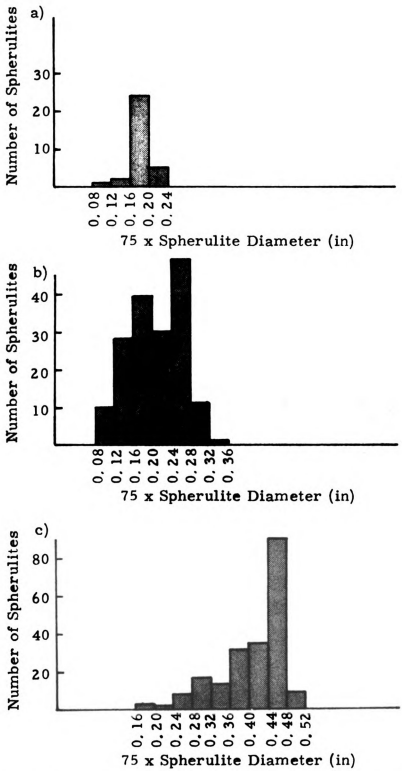

Figure A.4. Histograms of spherulites grown in 70-30-0.5 glass at 450°C for (a) 200 min., (b) 240 min., (c) 360 min., (d) 480 min., and (e) 600 min., after a nucleation heat treatment of 1 hour at 400°C.

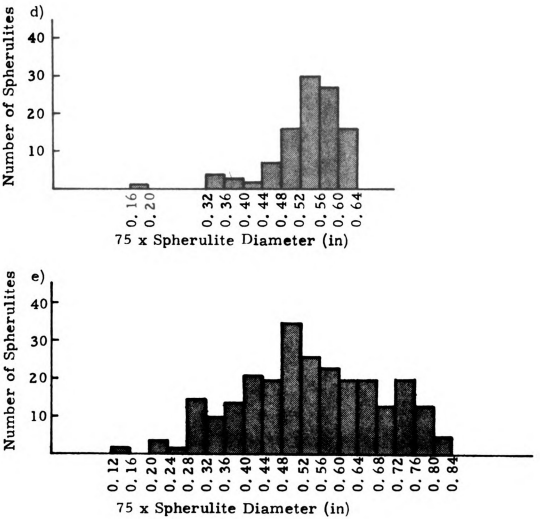

Figure A.4. cont.

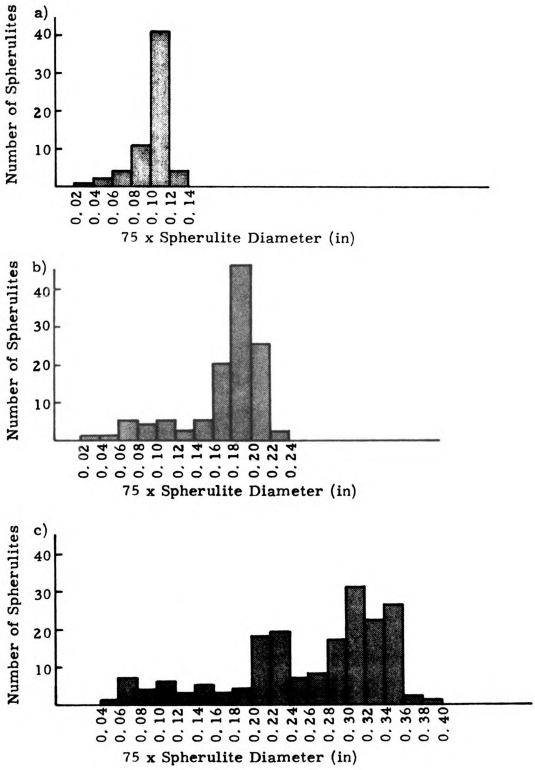

Figure A.5. Histograms of spherulites grown in 70-30-1.0 glass at 450°C for (a) 200 min., (b) 275 min., (c) 480 min., (d) 600 min., and (e) 720 min..

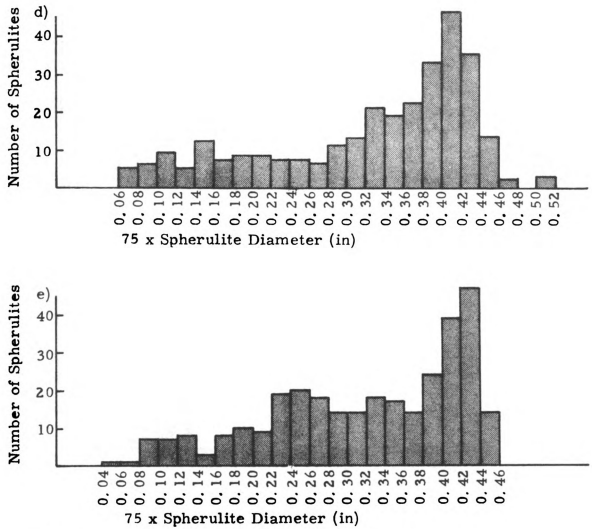

Figure A. 5. cont.

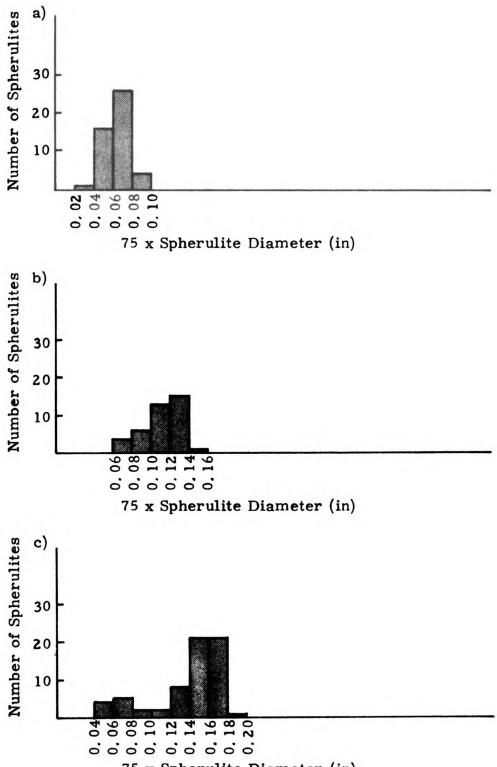

Figure A.6. Histograms of spherulites grown in 60-40-0.5 glass at 450°C for (a) 720 min., (b) 1080 min., and (c) 1405 min. after a nucleation heat treatment of 1 hour at 400°C; and for (d) 1440 min., (e) 1680 min., and (f) 1920 min. after a nucleation heat treatment of 6 hours at 400°C.

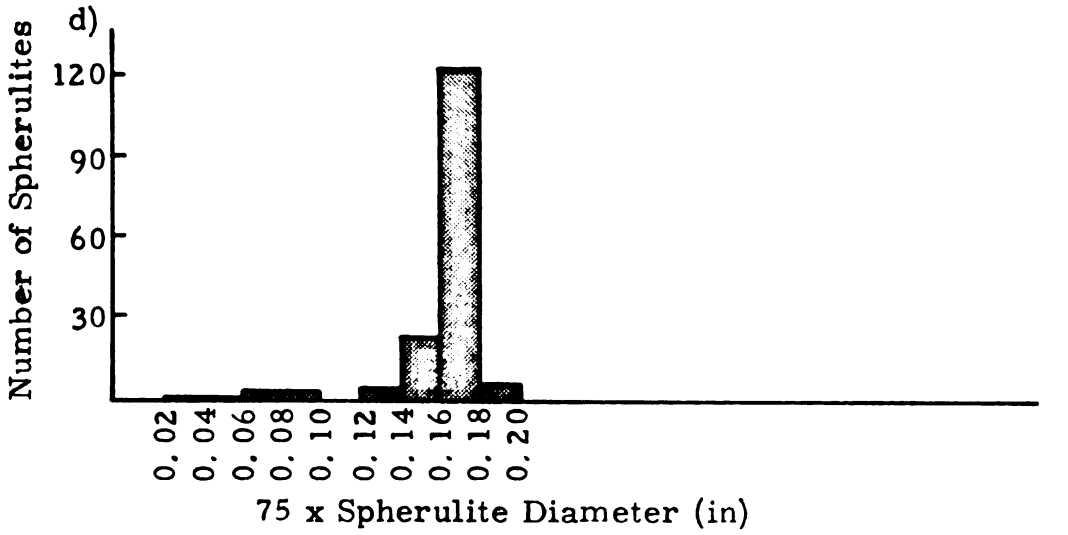

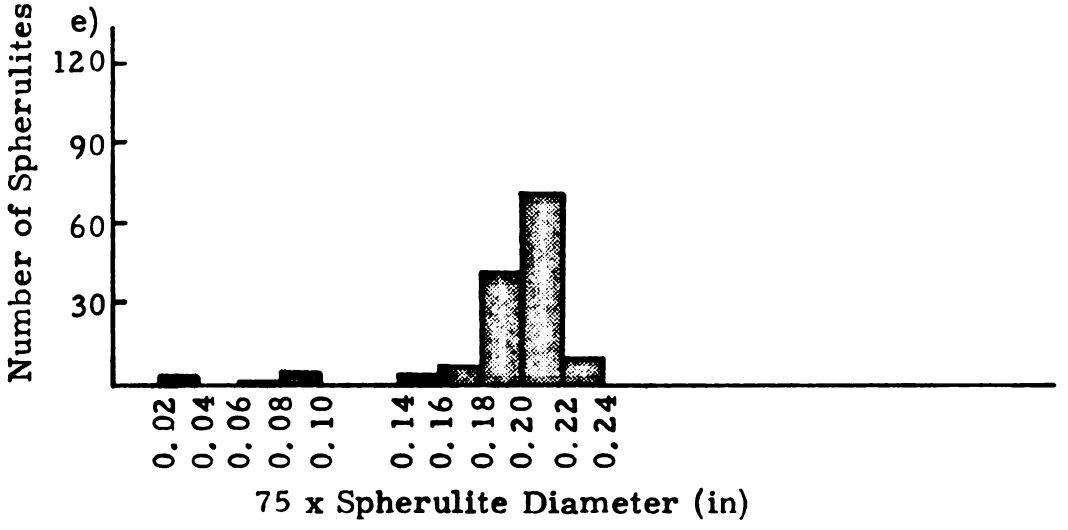

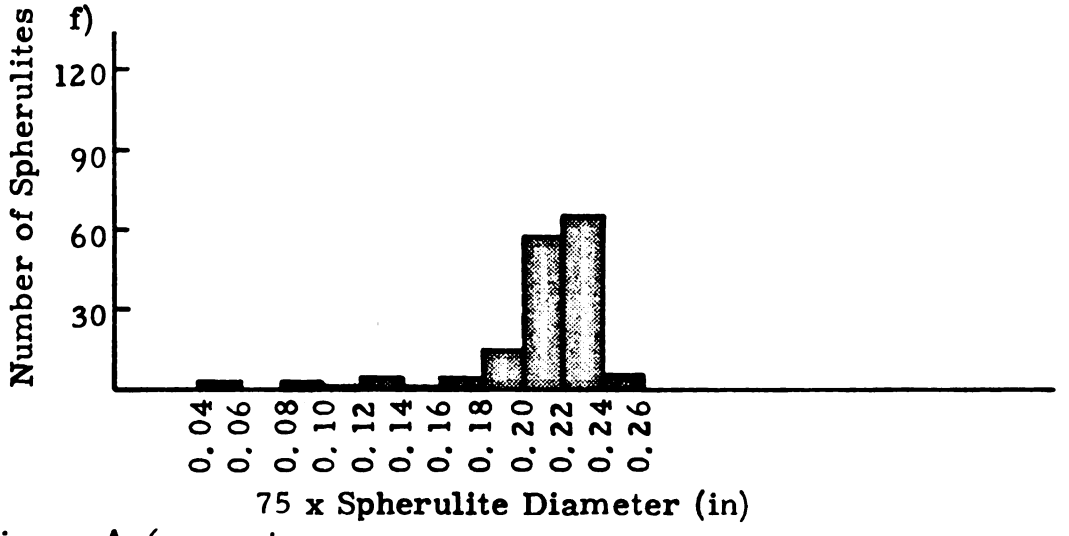

Figure A.6. cont.

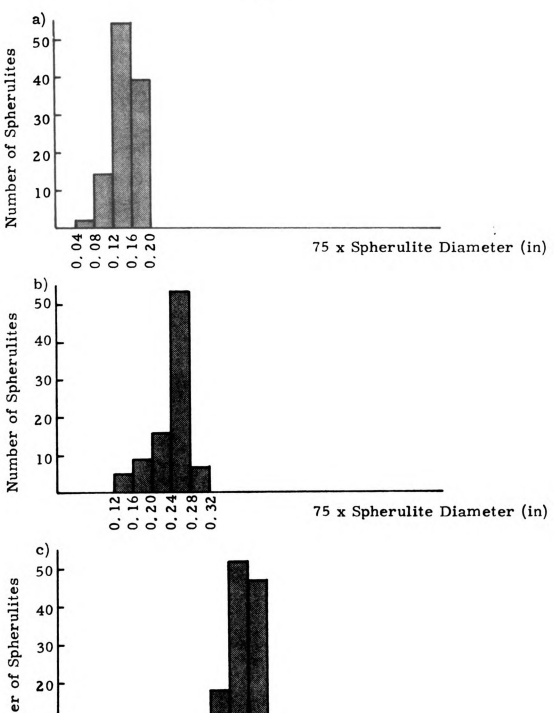

Figure A. 7. Histograms of spherulites grown in 70-30-0.5 glass at 500°C for (a) 10 min., (b) 15 min., (c) 22 min., (d) 30 min., and (e) 37 min., after a nucleation heat treatment of 1 hour at 400°C.

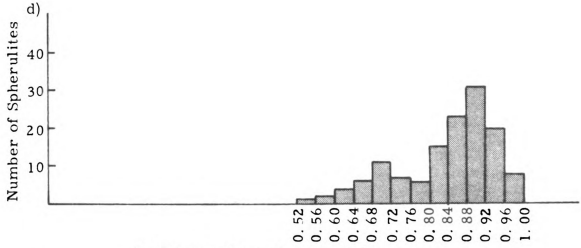

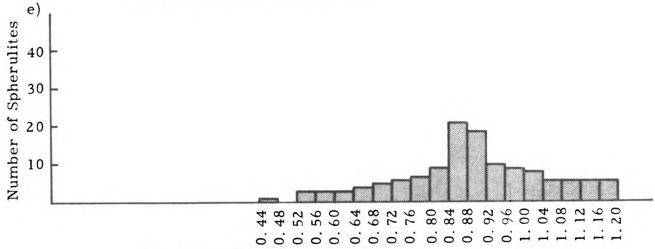

Figure A.7. cont.

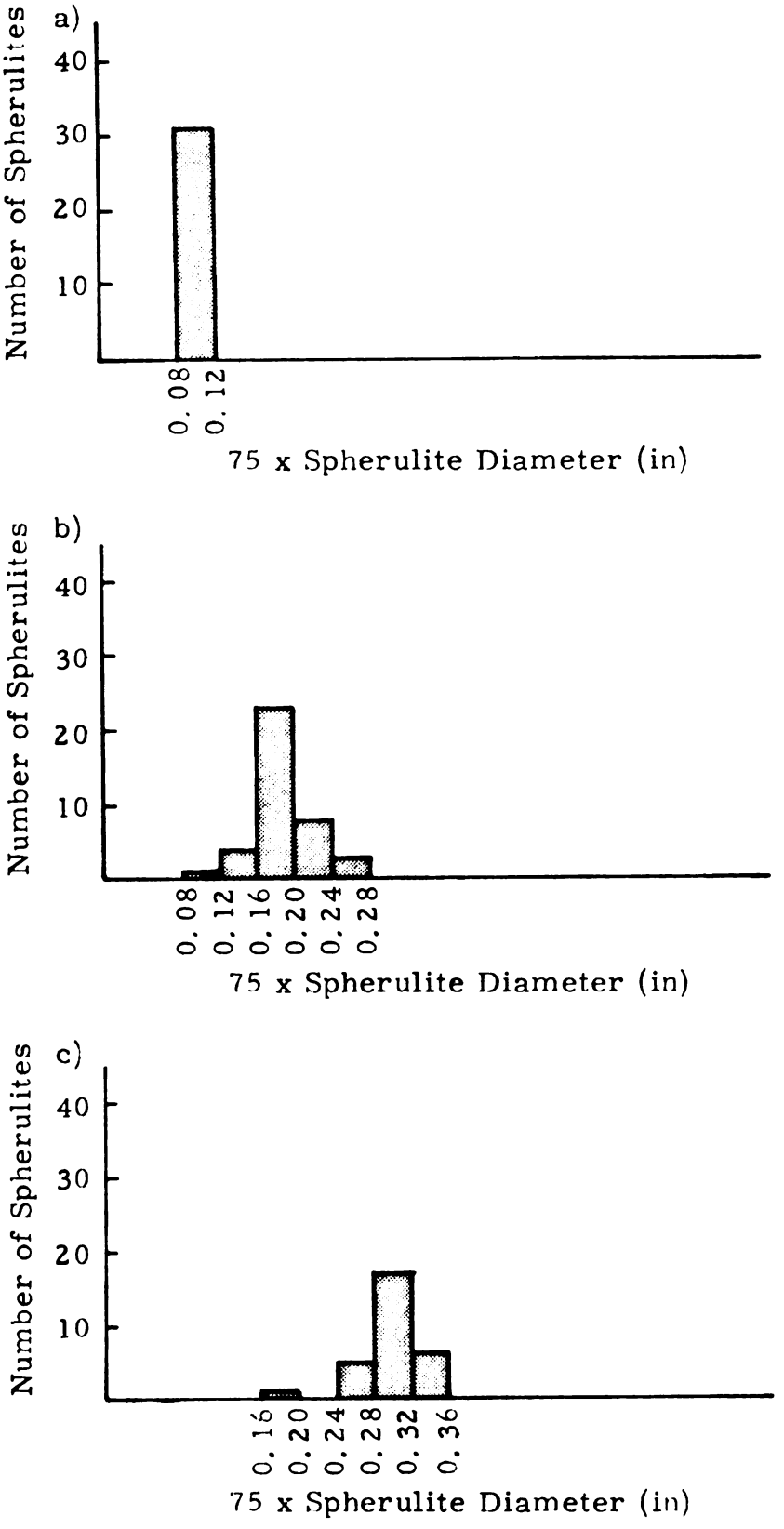

Figure A.8. Histograms of spherulites grown in 70-30-1.0 glass at 500°C for (a) 10 min., (b) 15 min., (c) 22 min., (d) 30 min., and (e) 37 min..

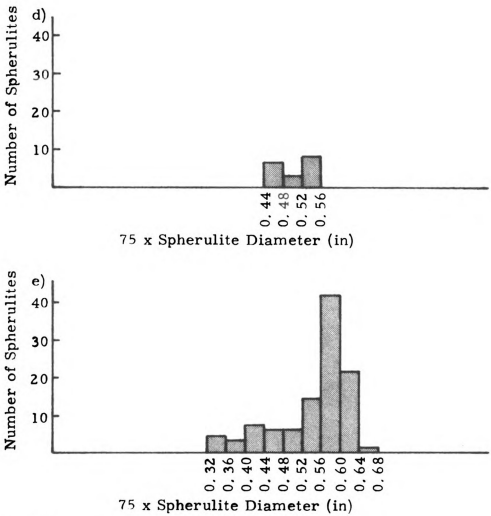

Figure A.8. cont.

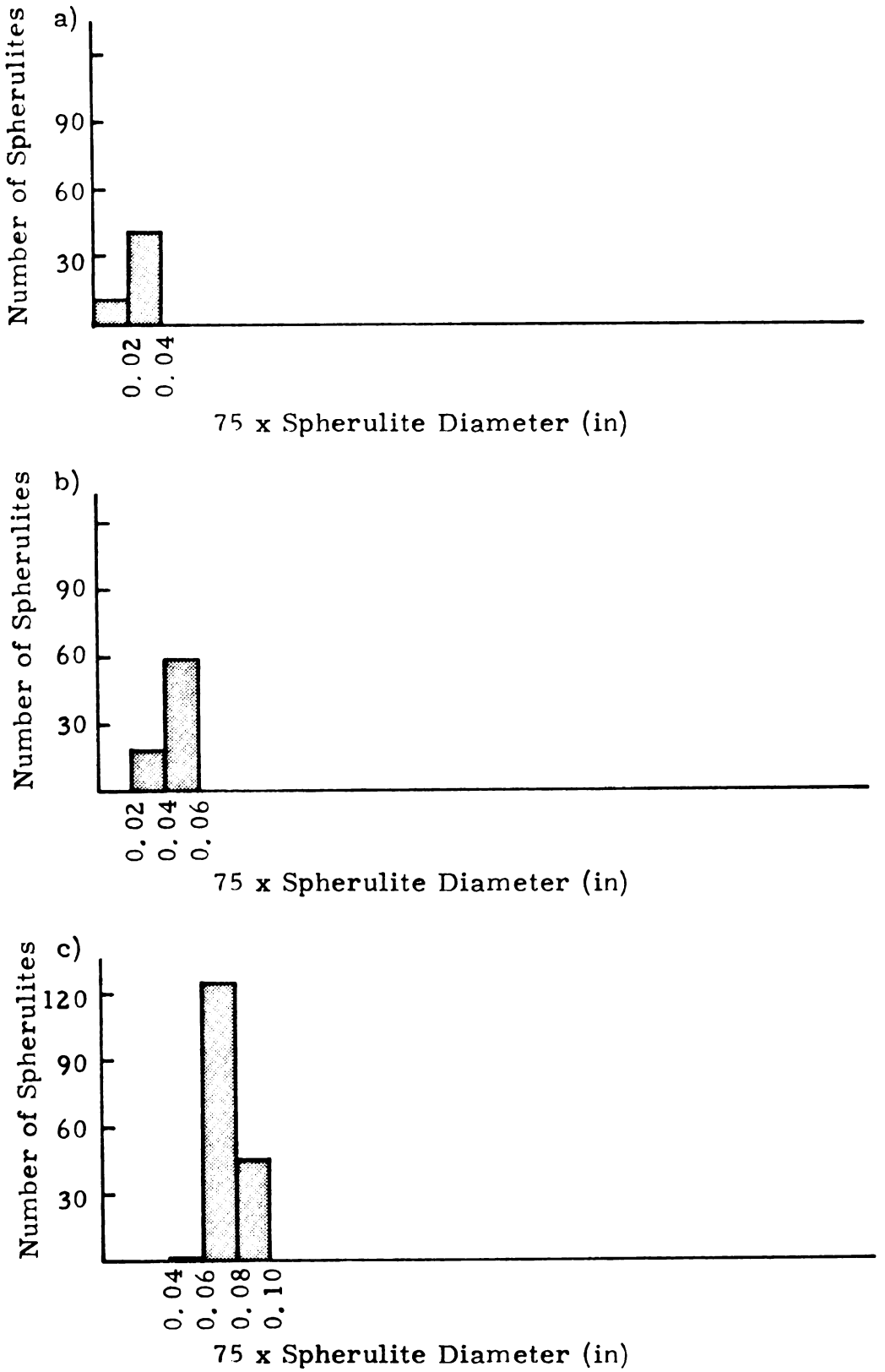

Figure A.9. Histograms of spherulites grown in 60-40-0.5 glass at 500°C for (a) 20 min., (b) 40 min., (c) 60 min., (d) 80 min., (e) 100 min., (f) 120 min., and (g)140 min., after a nucleation heat treatment of 6 hours at 400°C.

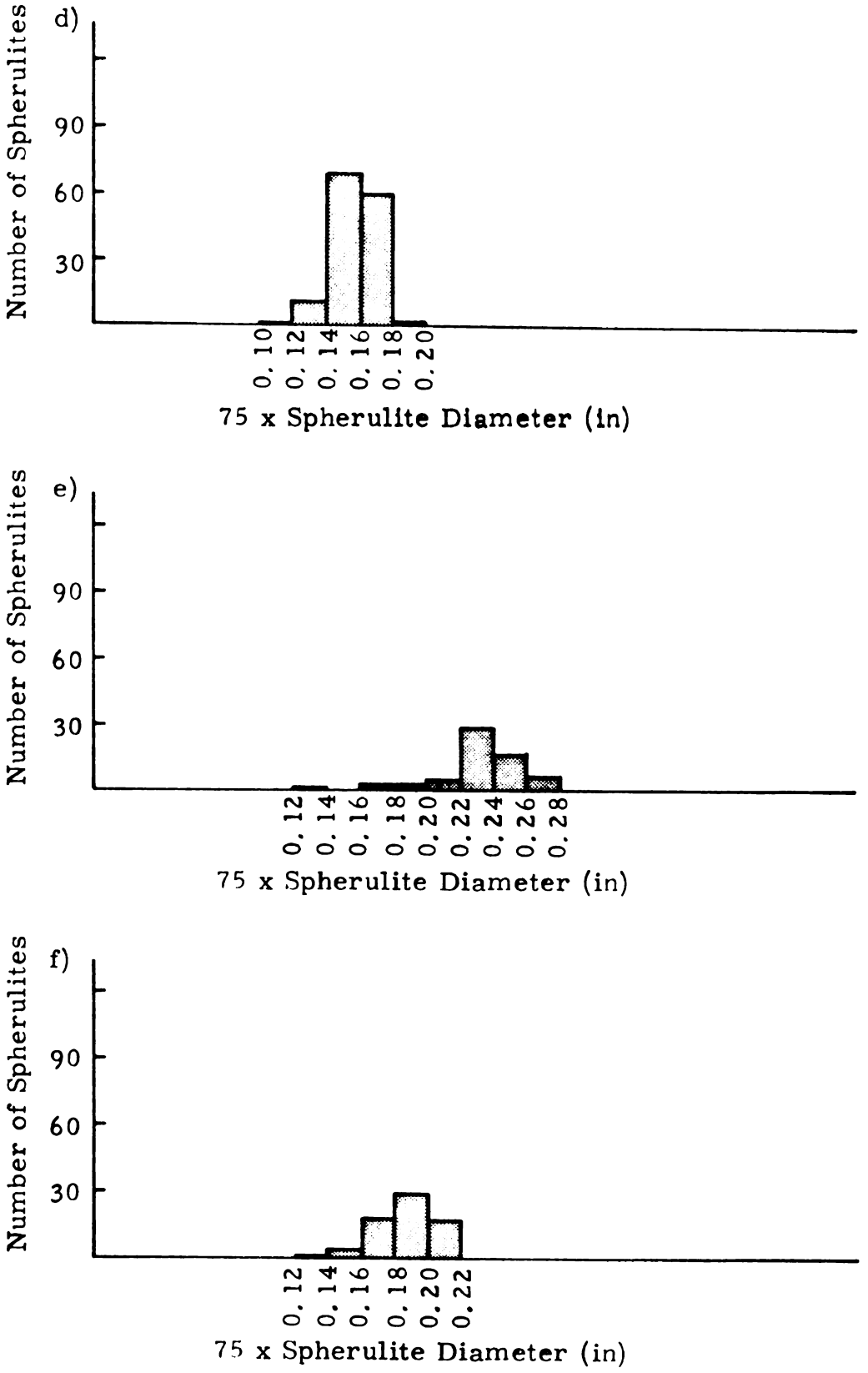

Figure A. 9. cont.

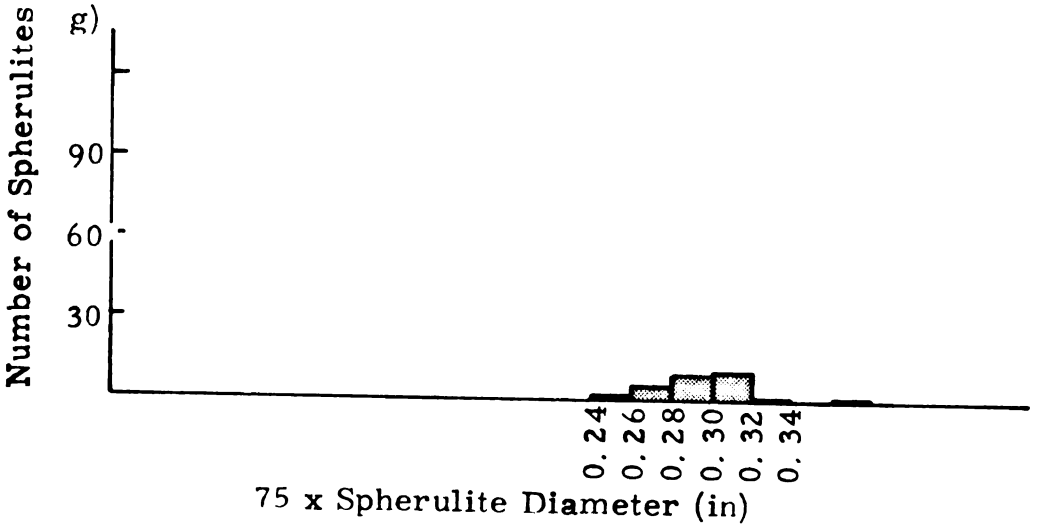

Figure A.9. cont.

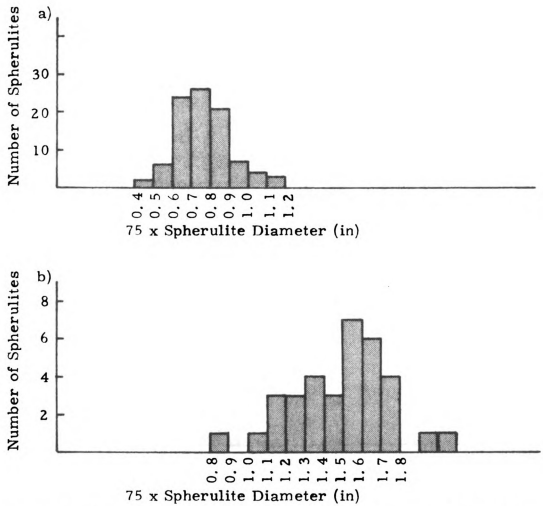

Figure A. 10. Histograms of spherulites grown in 70-30-0.5 glass at 550°C for (a) 3 min. and (b) 5 min., after a nucleation heat treatment of 1 hour at 400°C.

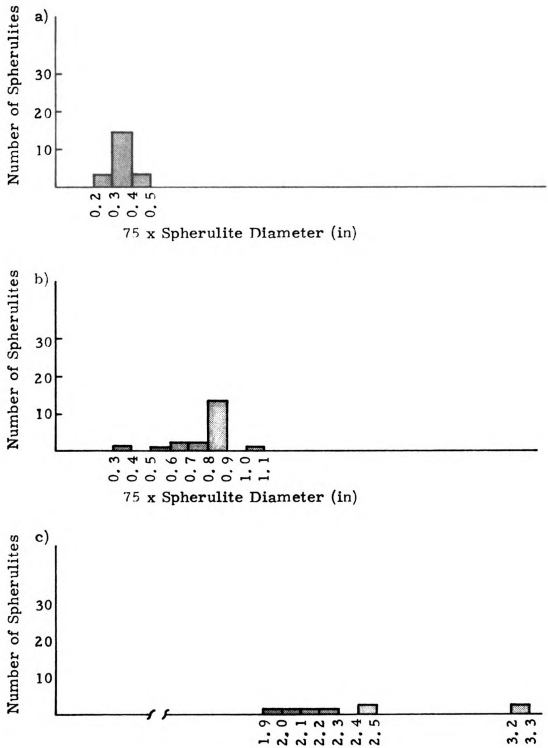

Figure A.11. Histograms of spherulites grown in 70-30-1.0 glass at 550°C for (a) 3 min., (b) 5 min., and (c) 10 min..

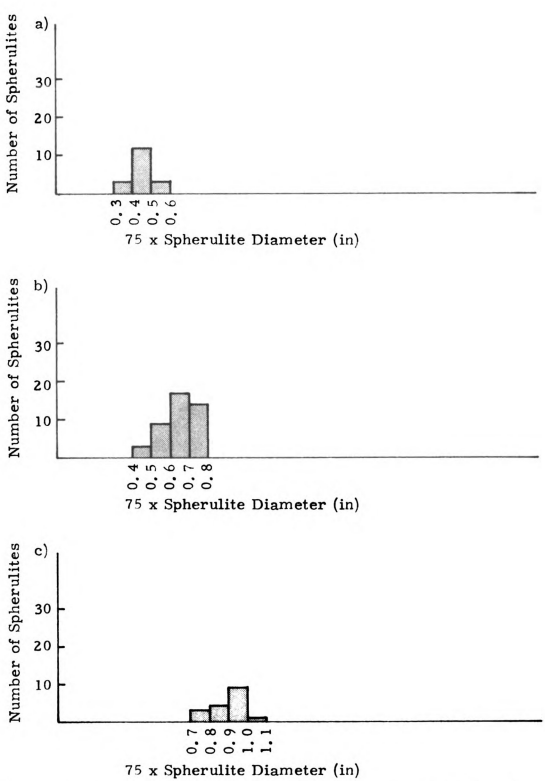

Figure A.12. Histograms of spherulites grown in 60-40-0.5 glass at 550°C for (a) 15 min., (b) 22 min., and (c) 30 min., after a nucleation heat treatment of 6 hours at 400°C.

LIST OF REFERENCES

1. N. M. Pavlushkin and G. P. Lisovskaya, Tr. Mosk. Khim. - Tekhnol. Inst. No. 55, 81(1967).

2. N. M. Pavlushkin and G. P. Lisovakaya, Steklo, 3, 114(1968).

3. N. M. Pavlushkin, L. S. Egorova, N. N. Kurtseva, and G. P. Lisovskaya, Eksp. Issled. Mineraloobrazov., Mater. Vses. Soveshch. Eksp. Tekh. Petrogr., 8th 1968, 169(1971).

4. Werner Vogel, Structure and Crystallization of Glasses, Pergamon Press, 1971.

5. R. R. Shaw and D. R. Uhlmann, J. Noncrystalline Solids, 1, 474(1969).

6. S. D. Stookey, in Ceramic Fabrication Processes, W. D. Kingery ed., The M. I. T. Press, Cambridge, 1958.

7. D. R. Uhlmann, in Materials Science Research, Vol. 4, T. J. Gray and V. D. Frechette eds., Plenum Press, New York, 1969.

8. G. O. Jones, Glass, Methuen, London, 1956.

9. J. W. Christian, The Theory of Transformations in Metals and Alloys, Pergamon Press, 1965.

10. R. Becker, Proceedings of the Physical Society of London, 52, 71(1940).

11. H. R. Swift, J. Am. Ceram. Soc., 30, 170(1947).

12. Robert H. Doremus, Glass Science, Wiley-Interscience, New York, 1973.

13. W. D. Scott and J. A. Pask, J. Am. Ceram. Soc., 44, 181(1961).

14. J. G. Morley, Glass Tech., 6, 77(1965).

15. Daniel R. Stewart, in Introduction to Glass Science, L. D. Pye,

H. J. Stevens, and W. C. LaCourse eds., Plenum Press, New York, 1972.

16. S. D. Stookey, Corning Research, 73(1961).

17. R. D. Maurer, J. Appl. Phys., 33, 2132(1962).

18. T. J. Barry, D. Clinton, L. A. Lay, R. A. Mercer, and R. P. Miller, J. Mat. Sci., 4, 596(1969).

19. T. J. Barry, D. Clinton, L. A. Lay, R. A. Mercer, and R. P. Miller, ibid., 5, 117(1970).

20. R. F. Geller, A. S. Creamer, and E. N. Bunting, J. Research Nat. Bur. Standards, 13, 237(1934).

21. H. C. Cooper, L. I. Shaw, and N. E. Loomis, Am. Chem. J., 42, 461(1909).

22. Siegfried Hilpert and Richard Nacken, Berichte. der Deut. Chem., 43, 2565(1910).

23. H. C. Cooper, E. H. Kraus, and A. A. Klein, Am. Chem. J., 47, 273(1912).

24. L. G. Berezkina and D. M. Chizhikov, Russ. J. Inorg. Chem., 7, 442(1962).

25. H. F. McMurdie and Elmer N. Bunting, J. Research Nat. Bur. Standards, 23, 543(1939).

26. J. F. Argyle and F. A. Hummel, J. Am. Ceram. Soc., 43, 452(1960).

27. E. V. Smirnova, in The Structure of Glass, Vol. 7, E. A. Porai-Koshits ed., Consultants Bureau, New York, 1966.

28. E. V. Smirnova, Izv. Akad. Nauk. SSSR, Neorg. Mater., 2, 2045(1966).

29. E. V. Smirnova, ibid., 3, 1230(1967).

30. W. Richard Ott and Malcolm G. McLaren, J. Am. Ceram. Soc., 53, 374(1970).

31. R. M. Smart and F. P. Glasser, ibid., 57, 378(1974).

32. R. A. Rita and C. G. Bergeron, ibid., 59, 274(1976).

33. T. F. Beals and W. C. Bigelow, in Symposium on Advances in Electron Metallography and Electron Probe Microanalysis, ASTM Spec. Tech. Publ. No. 317, 1962.

34. H. R. Limb, The Review of Scientific Instruments, 41, 874(1970).

35. H. W. Billhardt, The American Mineralogist, 54, 510(1969).

36. H. W. Billhardt, Glastech. Ber., 42, 498(1969).

37. D. G. Burnett and R. W. Douglas, Phys. Chem. Glasses, 12, 117(1971).

38. George J. Bair, J. Am. Ceram. Soc., 19, 339(1936).

39. P. F. James and S. R. Keown, Phil. Mag., Ser. 8, 30, 789(1974).

40. D. A. Jackson, in Liquid Metals and Solidification, ASM, Cleveland, 1958.

41. K. A. Jackson, in Growth and Perfection of Crystals, R. H. Doremus, B. W. Roberts, and D. Turnbull eds., Wiley, New York, 1958.

42. K. A. Jackson, in Progress in Solid State Chemistry, Vol. 4, H. Reiss ed., 1967.

43. Donald R. Uhlmann, in Advances in Nucleation and Crystallization in Glasses, American Ceramic Society, Columbus, 1972.

44. L. Shartsis and E. S. Newman, J. Am. Ceram. Soc., 31, 213 (1948).

45. H. D. Keith and F. J. Padden, Jr., J. Appl. Phys., 34, 2409 (1963).